JOURNAL OF PETROLOGY

Journal of Petrology, 2016, Vol. 57, No. 4, 655–684
doi: 10.1093/petrology/egw011
Advance Access Publication Date: 8 April 2016
Original Article

OXFORD

Mantle Recycling: Transition Zone Metamorphism of Tibetan Ophiolitic Peridotites and its Tectonic Implications

W. L. Griffin[1]*, J. C. Afonso[1], E. A. Belousova[1], S. E Gain[1], X.-H. Gong[2] J. M. González-Jiménez[1,3], D. Howell[1], J.-X. Huang[1,4], N. McGowan[1], N. J. Pearson[1], T. Satsukawa[1], R. Shi[1,2], P. Williams[5], Q. Xiong[1,6], J.-S. Yang[7], M. Zhang[1] and Suzanne Y. O'Reilly[1]

[1]ARC Centre of Excellence for Core to Crust Fluid Systems and GEMOC, Department of Earth and Planetary Sciences, Macquarie University, NSW 2109, Australia; [2]Key Laboratory of Continental Collision and Plateau Uplift, Institute of Tibetan Plateau Research, Chinese Academy of Sciences, Beijing 100101, China; [3]Departamento de Geología and Andean Geothermal Center of Excellence (CEGA), Facultad de Ciencias Físicas y Matemáticas, Universidad de Chile, Santiago, Chile; [4]State Key Laboratory of Lithospheric Evolution, Institute of Geology and Geophysics, Chinese Academy of Sciences, Beijing 100029, China; [5]School of Science and Health, University of Western Sydney, Locked Bag 1757, Penrith, NSW 2750, Australia; [6]State Key Laboratory of Geological Processes and Mineral Resources, School of Earth Sciences, China University of Geosciences, Wuhan 430074, China and [7]Institute of Geology, Chinese Academy of Geological Sciences, Beijing 100037, China

*Corresponding author. Telephone: +61 02 98508954. Fax: +61 02 98508943.
E-mail: bill.griffin@mq.edu.au.

Received October 18, 2015; Accepted February 25, 2016

ABSTRACT

Large peridotite massifs are scattered along the 1500 km length of the Yarlung–Zangbo Suture Zone (southern Tibet, China), the major suture between Asia and Greater India. Diamonds occur in the peridotites and chromitites of several massifs, together with an extensive suite of trace phases that indicate extremely low fO_2 (SiC, nitrides, carbides, native elements) and/or ultrahigh pressures (UHP) (diamond, TiO_2 II, coesite, possible stishovite). New physical and isotopic (C, N) studies of the diamonds indicate that they are natural, crystallized in a disequilibrium, high-*T* environment, and spent only a short time at mantle temperatures before exhumation and cooling. These constraints are difficult to reconcile with previous models for the history of the diamond-bearing rocks. Possible evidence for metamorphism in or near the upper part of the Transition Zone includes the following: (1) chromite (in disseminated, nodular and massive chromitites) containing exsolved pyroxenes and coesite, suggesting inversion from a high-*P* polymorph of chromite; (2) microstructural studies suggesting that the chromitites recrystallized from fine-grained, highly deformed mixtures of wadsleyite and an octahedral polymorph of chromite; (3) a new cubic Mg-silicate, with the space group of ringwoodite but an inverse-spinel structure (all Si in octahedral coordination); (4) harzburgites with coarsely vermicular symplectites of opx + Cr–Al spinel ± cpx; reconstructions suggest that these are the breakdown products of majoritic garnets, with estimated minimum pressures to > 13 GPa. Evidence for a shallow pre-metamorphic origin for the chromitites and peridotites includes the following: (1) trace-element data showing that the chromitites are typical of suprasubduction-zone (SSZ) chromitites formed by magma mixing or mingling, consistent with Hf-isotope data from magmatic (375 Ma) zircons in the chromitites; (2) the composition of the new cubic Mg-silicate, which suggests a low-*P* origin as antigorite, subsequently dehydrated; (3) the peridotites themselves, which carry the trace element signature of metasomatism in an SSZ environment, a signature that must have been imposed before the incorporation of the UHP and low-fO_2 phases. A proposed *P–T–t* path involves the original formation of chromitites in mantle-wedge

harzburgites, subduction of these harzburgites at *c*. 375 Ma, residence in the upper Transition Zone for >200 Myr, and rapid exhumation at *c*. 170–150 Ma or 130–120 Ma. Os-isotope data suggest that the subducted mantle consisted of previously depleted subcontinental lithosphere, dragged down by a subducting oceanic slab. Thermomechanical modeling shows that roll-back of a (much later) subducting slab would produce a high-velocity channelized upwelling that could exhume the buoyant harzburgites (and their chromitites) from the Transition Zone in < 10 Myr. This rapid upwelling, which may explain some characteristics of the diamonds, appears to have brought some massifs to the surface in forearc or back-arc basins, where they provided a basement for oceanic crust. This model can reconcile many apparently contradictory petrological and geological datasets. It also defines an important, previously unrecognized geodynamic process that may have operated along other large suture zones such as the Urals.

Key words: Transition Zone; Tibet collision zone; UHP and super-reducing conditions; Yarlung–Zangbo Suture Zone; geodynamic exhumation; mantle recycling

GEOLOGICAL SETTING AND INTRODUCTION TO THE PROBLEM

The Yarlung–Zangbo Suture Zone (YZSZ) is one of the great tectonic scars on the face of the Earth; it runs roughly east–west at *c*. 29°N, for 1500 km across the southern edge of Tibet (Fig. 1). It is commonly regarded as marking the locus of the final plate collision between India and Asia, and is part of a still longer zone of sutures that extends westward to Turkey, marking the closure of first the Paleo-Tethys (Early Devonian–Early Permian) and then the Meso-Tethys and Neo-Tethys (Triassic–Cretaceous) oceans [see summaries by Metcalfe (1996) and Moghadam *et al*. (2015)]. At least three subparallel sutures, related to earlier stages of ocean closure and transcurrent faulting, lie farther north, dividing the Tibetan Plateau into several parallel terranes.

The YZSZ separates the continental (Middle Proterozoic–Early Paleozoic) Lhasa block to the north from a series of Greater India-derived terranes to the south, making up the Himalayan domain. The southern edge of the Lhasa block is dominated by plutonic rocks of the Gangdese Batholith (>150 Ma to 35 Ma; Murphy *et al*., 1997; Harrison *et al*., 2000). These are commonly interpreted as arc magmas, related to the complex northward subduction of the Neo-Tethys oceanic plate. The sedimentary, volcanic and ultramafic rocks of the YZSZ, which range mainly from Triassic to Cretaceous in age, make up the deformed remnants of the Neo-Tethys domain; they were first obducted southward either onto the continental margin of northern India or onto a series of intra-oceanic island arcs, and later thrust to the north during the Cenozoic collision between India and Asia (Aitchison *et al*., 2002, 2003, 2007*a*). Final southward thrusting produced thick zones of serpentinite mélange along the southern contacts of the peridotites with Triassic or younger sediments in many areas.

A major feature of the YZSZ is a discontinuous line of tectonically emplaced peridotite massifs. Some are up to 700 km^2 in area (2000–3000 km^3), whereas others are thin slivers (Fig. 1; Table 1). Similar peridotite massifs occur within the subparallel sutures further to the north on the Tibetan Plateau (Fig. 1). Several of these massifs consist largely of highly depleted harzburgites (Table 1); their compositions can be modeled as residues after as much as 30–40% partial melting of a primitive mantle (Dubois-Cote *et al*., 2005; Xiong, 2015). Some of these also contain numerous bodies of dunite, which locally enclose podiform chromitites up to commercial scales. Other massifs or ultramafic domains are more typically lherzolitic, consistent with 7–12% partial melting (Dubois-Cote *et al*., 2005; Hebert *et al*., 2012; Xiong, 2015). Many of the more depleted bodies have been regarded as Jurassic in age because they are spatially associated with mafic rocks of that age; the remainder, including most of the less depleted bodies, are considered to have been emplaced in Cretaceous times (Xiong *et al*., 2016). More detailed considerations on the geological setting are given below.

Some of the massifs contain both depleted and 'fertile' rocks; relationships have been described as 'gradational' in some areas (Nicolas *et al*., 1981; Wang *et al*., 1987; Girardeau & Mercier, 1988), but may be tectonic in others. Some of the controversies in the literature may arise from a situation in which different research groups have sampled different rock types within a given massif, but applied their results to the whole massif. Many typical ophiolitic mantle sections worldwide contain abundant primary hydrous minerals (e.g. Kempirsai in Kazakhstan, Mayari–Baracoa in Cuba; Melcher *et al*., 1997; Proenza *et al*., 1999) and also are heavily serpentinized, reflecting H_2O circulation at spreading centers and in suprasubduction-zone (SSZ) systems. In contrast, many of the YZSZ bodies (especially the larger ones) are strikingly fresh, except in tectonized zones related to emplacement.

The origins of the YZSZ peridotites have become even more enigmatic, and models for their genesis increasingly diverse, as reports have accumulated on an extensive assortment of unusual trace minerals (Supplementary Data Table A1; supplementary data are available for downloading at http:/www.petrology.oxfordjournals.org; see summaries by Robinson *et al*.,

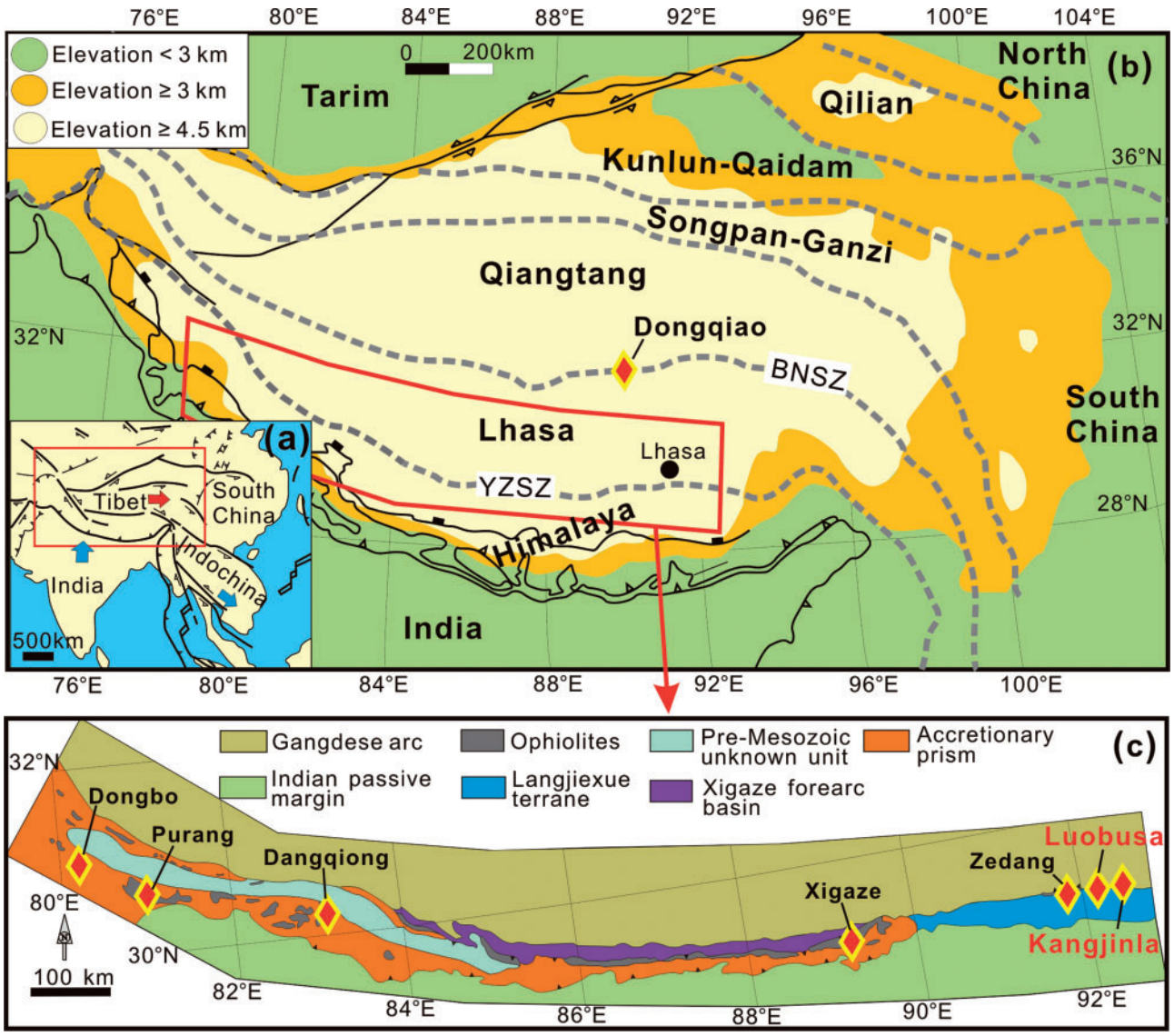

Fig. 1. Location maps. (a) Situation of Tibet within Asia. (b) Overview of Tibet, showing the Yarlung–Zangbo Suture Zone (YZSZ) and Bangong–Nujiang Suture Zone (BNSZ); names of blocks or terranes are shown in black; red outline shows the location of (c), a more detailed map of the Yarlung Zangbo Suture Zone, showing the locations of the peridotite massifs ('ophiolites') discussed here. Yellow–red diamonds show localities where diamonds have been reported from chromitites and/or peridotites (see Supplementary Data Table A1).

2004; Xu *et al.*, 2015) separated originally from chromitites, but more recently also from the host peridotites (Yang *et al.*, 2014). Some of these phases (diamond, TiO_2 II, coesite, stishovite pseudomorph) indicate ultrahigh-pressure (UHP, $\geq$4 GPa) conditions; others (native elements, alloys, carbides, nitrides) suggest very low fO_2 conditions (Dobrzhinetskaya *et al.*, 2009; Green, 2012). We refer to these collectively as the 'super-reducing, ultrahigh-pressure' or 'SuR-UHP' assemblage (Griffin *et al.*, 2013); this does not imply that all of the described phases coexisted as an equilibrium phase assemblage.

Few of the trace minerals reported from the chromites and peridotites have been seen *in situ*; the main exceptions are diamond, moissanite (SiC) and corundum (Xu *et al.*, 2009, 2015; Liang *et al.*, 2014; J.-Q. Liu, personal communication). The paragenetic relationships of most SuR-UHP phases thus are largely unknown or, in the case of diamonds and SiC, they are surrounded by 'amorphous carbon' (Yang *et al.*, 2014; see below), and are not clearly understood. Most have been recovered after crushing very large (up to 1100 kg) samples in commercial-scale plants, followed by magnetic and heavy-liquid separation (Xu *et al.*, 2009, 2015). This makes it difficult to determine their context, and has led to some skepticism in the research community regarding their significance, or even their natural occurrence.

Here we integrate new data and interpretations with a number of recent key developments, based on field observations and detailed studies of small samples. We present an evolutionary model that is consistent with

Table 1: Summary of the features of the main peridotite massifs in the YZSZ, south Tibet (China)

Name	Sub-unit	Latitude (N)	Longitude (E)	Size (km^2)	Major lithology*	Chromitite deposit	Ages of relevant mafic rocks (methods; references)
Luobusa	Kangjinla, Xiangkashan, Luobusa	29°07·5′–29°11·0′	92°09·0′–92°30·5′	~70	H, L	Large	177 Ma (Sm–Nd isochron; Zhou et al., 2002) 163 Ma (zircon U–Pb; Zhong et al., 2006) 148–150 Ma (zircon U–Pb; Chan et al., 2015) 128–130 Ma (zircon U–Pb; Wu et al., 2014)
Zedang†		29°15·0′–29°13·2′	91°33·0′–91°49·5′	~65	H, L	Small	273 Ma (zircon U–Pb; McDermid et al., 2002) 175 Ma (Sm–Nd isochron; Wei et al., 2006) 130–138, 155 Ma (zircon U–Pb; Liu et al., 2013; Wu et al., 2014)
E. Xigaze	Renbu, Dazhuqu, Bailang, Deji, Luqu	29°07·5′–29°15·0′	88°43·0′–89°17·0′	~400	H, L	Small (only in Renbu)	125–130 Ma (zircon U–Pb; Malpas et al., 2003; Li et al., 2009; Dai et al., 2013; Wu et al., 2014) 124–127 Ma (amphibole Ar–Ar; Guilmette et al., 2009)
W. Xigaze	Qumei Jiding Ang-ren	29°08·0′–29°19·0′	86°57·0′–88°40·0′	~600	H, L	Rare	124–132 Ma (zircon U–Pb; Wang et al. 2006; Dai et al., 2013; Chan et al., 2015) 27 Ma (amphibole Ar–Ar; Guilmette et al. 2009)
Sangsang		29°08·0′–29°53·0′	86°33·0′–86°54·0′	~90	H, L	No	125 Ma (Zircon U–Pb; Xia et al., 2008)
Saga		29°32·0′–29°41·0′	84°57·0′–85°20·0′	~90	H, L	No	124–129 Ma (amphibole Ar-Ar; Guilmette *et al.*, 2012)
Zhongba		29°44·5′–29°47·0′	83°46·5′–83°50·0′	~10	H	No	126 Ma (zircon U–Pb; Dai et al., 2012)
Xiugugabu	Including Dangqiong	30°11·5′–30°53·0′	82°25·0′–83°14·0′	~700	H, L	Rare	122–127 Ma (zircon U–Pb; Chan et al., 2015)
Purang‡		30°35·6′–30°45·5′	80°42·0′–81°24·0′	~600	H, L	Rare	119–130 Ma (zircon U–Pb; Liu et al., 2011; Chan et al., 2015)
Dongbo§		30°55·0′–31°10·0′	80°00·0′–80°20·0′	~414	H	Rare	128–130 Ma (zircon U–Pb; Xiong et al., 2011) 160 Ma (zircon U–Pb; Chan et al., 2015)

*H, harzburgite; L, lherzolite.
†Alternative name 'Zedong'.
‡Alternative name 'Yungbwa'.
§Alternative name 'Kiogar'.

results from thermomechanical simulations of collisional tectonics, and with available mineralogical, geochemical and chronological constraints. This model may help to explain the history of these enigmatic peridotites and resolve problems raised by other studies. Our results define a globally significant process of lithospheric mantle recycling that may have occurred in other collision zones of comparable magnitude.

SUMMARY OF EVIDENCE, AND A *P–T–t* PATH

We argue that at least some of the YZSZ harzburgites represent lithospheric mantle that was initially modified at shallow depths in an SSZ environment, subducted into the Transition Zone (~410–660 km depth) and then (much later) re-exhumed, perhaps to the sea floor [see also Green (2012)]. Several lines of evidence can be used to constrain the *P–T–t* history of these bodies.

Evidence for Transition Zone metamorphic conditions

Chromitites and their inclusions

Whereas diamonds, suggesting depths of > 150 km, have been known from the chromitites of the Luobusa massif for at least 30 years, the first evidence of a potentially deeper origin was from the description (Yang *et al.*, 2007) of a reaction zone of acicular kyanite and SiO_2 between a silicate matrix and a spherical grain of Fe–Ti alloy separated from a chromitite. The SiO_2 blades are now granular aggregates of coesite, and have been interpreted as pseudomorphs after stishovite (>300 km). Transmission electron microscope (TEM) studies of the same grain (Dobrzhinetskaya *et al.*, 2009) identified nano-phases of TiO_2 II, indicating depths similar to those required for formation of stishovite, as well as TiN and BN. Dobrzhinetskaya *et al.* (2009), Ruskov *et al.* (2010) and McGowan *et al.* (2015) have used Møssbauer spectrometry to show that the spinels in massive chromitites from Luobusa have high Fe^{3+} contents, although they also contain abundant spherules of native Fe (Fig. 2). This combination of phases probably represents the high-*P* disproportionation of $Fe^{2+} \rightarrow Fe^{3+} + Fe^0$ predicted for the deep mantle (Frost *et al.*, 2004; McCammon, 2005). Although the reaction itself is difficult to quantify in terms of depth, Rohrbach *et al.* (2007) suggested that the high Fe^{3+} in the Luobusa chromites indicates that they were in the structure of the Ca-ferrite-structured polymorph, requiring deep-mantle conditions (see discussion below).

Yamamoto *et al.* (2009) showed that chromite grains in some massive and nodular chromitites from the Luobusa body (orebody #31) contain abundant needles of SiO_2, diopside and more rarely enstatite, with preferred crystallographic orientations (Fig. 3); TEM studies showed that at least some of the SiO_2 needles are coesite. Yamamoto *et al.* (2009) suggested that because Ca and Si are essentially insoluble in the cubic chromite structure, this exsolution implies inversion from the higher-pressure Ca-ferrite structure. This orthorhombic polymorph of chromite can in principle accommodate ions such as Ca and Si; it was first recognized in meteorites, coexisting with ringwoodite, and was later synthesized by Chen *et al.* (2003). Ca and Si would have been available for uptake in the Ca-ferrite structure, as clinopyroxene is a common interstitial phase in the chromitites (Fig. 3a). Recent syntheses using Luobusa chromitites as starting materials have found that levels of Ca and Si begin to increase with *P* at *c.* 12 GPa (1200–1400°C), peaking at levels of 1–3% of each element at around 14 GPa, and dropping as the chromite goes to the higher-*P* CT structure (Wu *et al.*, 2011; Zhang & Jin, in preparation). Arai (2013) has suggested that the Si and Ca were derived from low-*T* inclusions of amphibole, but there is little doubt that the concentrations of these elements in the high-*P* chromitites were controlled by equilibrium with diopside.

We have now identified the above type of exsolution in chromite from several other chromitite bodies within the Luobusa–Kangjinla massif. Our observation of similar needles in massive, nodular and coarse-grained disseminated chromite (Fig. 3) indicates that all types of chromite at Luobusa–Kangjinla have experienced a common *P–T* history. Relatively large (5 μm) diopside needles in chromite have compositions (Table 2) similar to those of large (up to 200 μm) abundant euhedral diopside crystals (Fig. 3a) separated from the same samples, suggesting equilibration during exsolution. This is consistent with the equilibrated near-equigranular microstructures with 120° triple junctions, smooth and nearly straight grain boundaries, and relatively low mean misorientation per grain, which are seen in many samples of massive chromitite in which this type of exsolution is observed (Satsukawa *et al.*, 2015; Fig. 4).

It is noteworthy that in the nodular chromitites, single nodules typically consist of a few large crystals in microstructural equilibrium (Fig. 3c). This is strikingly different from the fine-grained olivine–chromite aggregates that make up most nodular chromitites in typical ophiolites. Pritchard *et al.* (2015) have shown that such nodules begin with the nucleation and rapid growth of skeletal crystals of chromite, trapping silicate melt; these nuclei are overgrown epitaxially by more euhedral crystals to form the nodules. We interpret the coarsely crystalline nature of the Tibetan chromite nodules as reflecting high-*T* recrystallization, perhaps during inversion from the higher-*P* polymorphs.

Satsukawa *et al.* (2015) applied electron backscattered diffraction (EBSD) analysis to a massive chromitite from the Kanjingla area (orebody #11), which has an equilibrated near-equigranular microstructure and extensive exsolution. Many small (median diameter *c.* 50 μm) olivine grains are included within the chromite; larger (median *c.* 200 μm) olivine grains occur between the large chromite grains (Fig. 4). Exsolved diopside needles occur in irregular areas in the cores of chromite grains, and the chromite grains show a clear crystallographic preferred orientation (CPO; Fig. 4d). Such a CPO

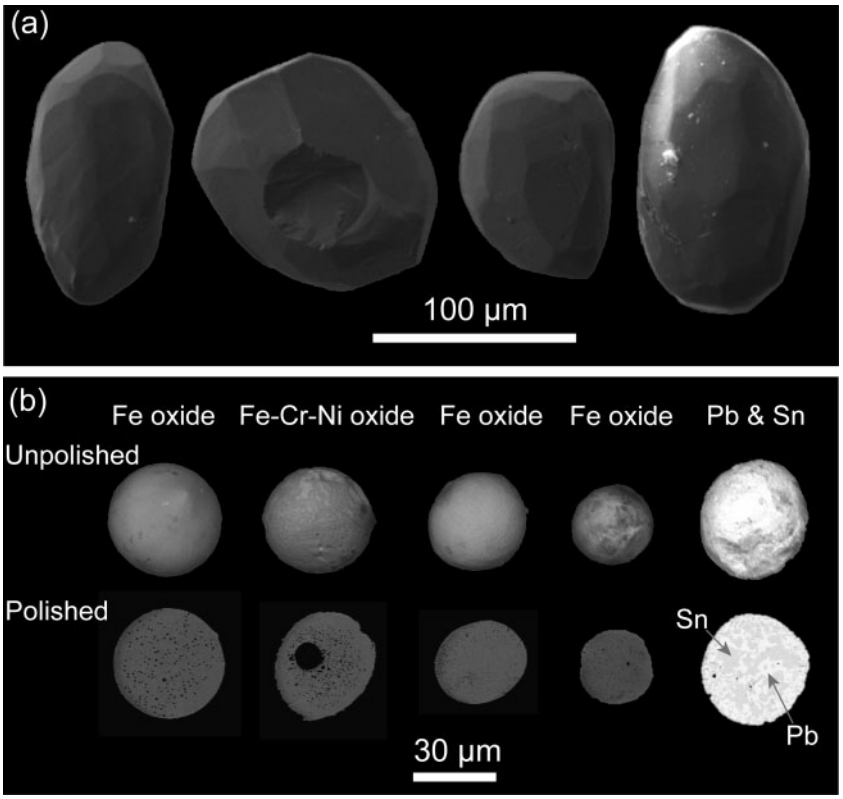

Fig. 2. Phases separated from Luobusa massive chromitites; analyses are given in Table 2. (a) SEM images of diopside grains showing facets imposed by microstructural equilibrium with chromite; (b) SEM images of spherules of native Fe (locally rimmed by wüstite) and alloys, and BSE images of polished sections of each grain. The four dark grains are Fe; the 'frothy' nature of the first two should be noted. Dark 'holes' are a Cr oxide. The light grain is an intergrowth of Pb and Sn in roughly equal proportions.

does not resemble typical deformation- or growth-induced textures known from cubic phases. In contrast, the patterns resemble nearly point-maximum concentrations, which could be produced by crystal-plastic deformation or recrystallization of a phase with the orthorhombic (CF) structure; this implies that the CPO was preserved during the inversion to the lower-pressure cubic chromite structure. The zoning in the abundance of exsolved needles (Fig. 4a) suggests that grain growth accompanying or following the orthorhombic–cubic inversion expelled the exsolved phases to the grain boundaries, but left the CPO (lineation) intact.

In the same sample, the olivine grains (both included and interstitial) also have a strong CPO, produced by dislocation creep, that defines a foliation and a lineation parallel to the [001] axis of the enclosing chromite. Analysis of subgrain-boundary misorientation defines the slip system as (010)[001], which is interpreted to have originated from deformation by dislocation creep within the mantle Transition Zone, and indicates that the observed (010)[001] fabric preserves the original (011)[100] fabric of wadsleyite (Satsukawa *et al.*, 2015, and references therein). These analyses strongly suggest that the current chromite–olivine assemblages were originally relatively fine-grained, strongly foliated and lineated aggregates of wadsleyite and CF-structured chromite, which experienced decompression into the olivine–chromite stability field with a minimum of deformation, but at temperatures high enough to promote grain growth in the chromite.

Numerous octahedral grains (50–200 μm; Fig. 5) made up of clinochlore, lizardite (Yang *et al.*, 1981) or antigorite (Table 3) have been separated from the chromitites of orebody #31 (Luobusa), and have been referred to as 'pseudomorphs after cubic olivine' (Robinson *et al.*, 2004). Most such grains are cloudy to opaque, but re-examination of transparent grains has resulted in the recognition of a new mineral, provisionally termed 'BWJ'. The detailed description of this new phase will be presented elsewhere; crystallographic data are summarized in Supplementary Data Table A2, and its chemical composition is given in Table 3. BWJ has a cubic structure analogous to that of ringwoodite, but is an inverse spinel, with all Si in octahedral coordination, rather than in the tetrahedral position as in a cubic spinel structure. However, the composition of BWJ is not quite that of olivine; it has a small excess of Si and a deficit of Mg, as well as small amounts of Al, and is the anhydrous analogue of antigorite (Table 3). BWJ has not been identified *in situ*, but chromite grains with abundant exsolution needles commonly contain numerous grains of the same shape and size (Fig. 5c), now replaced by aggregates of antigorite; their compositions are consistent with hydration of the BWJ phase (Table 3). In some samples these pseudomorphs define rough linear arrays.

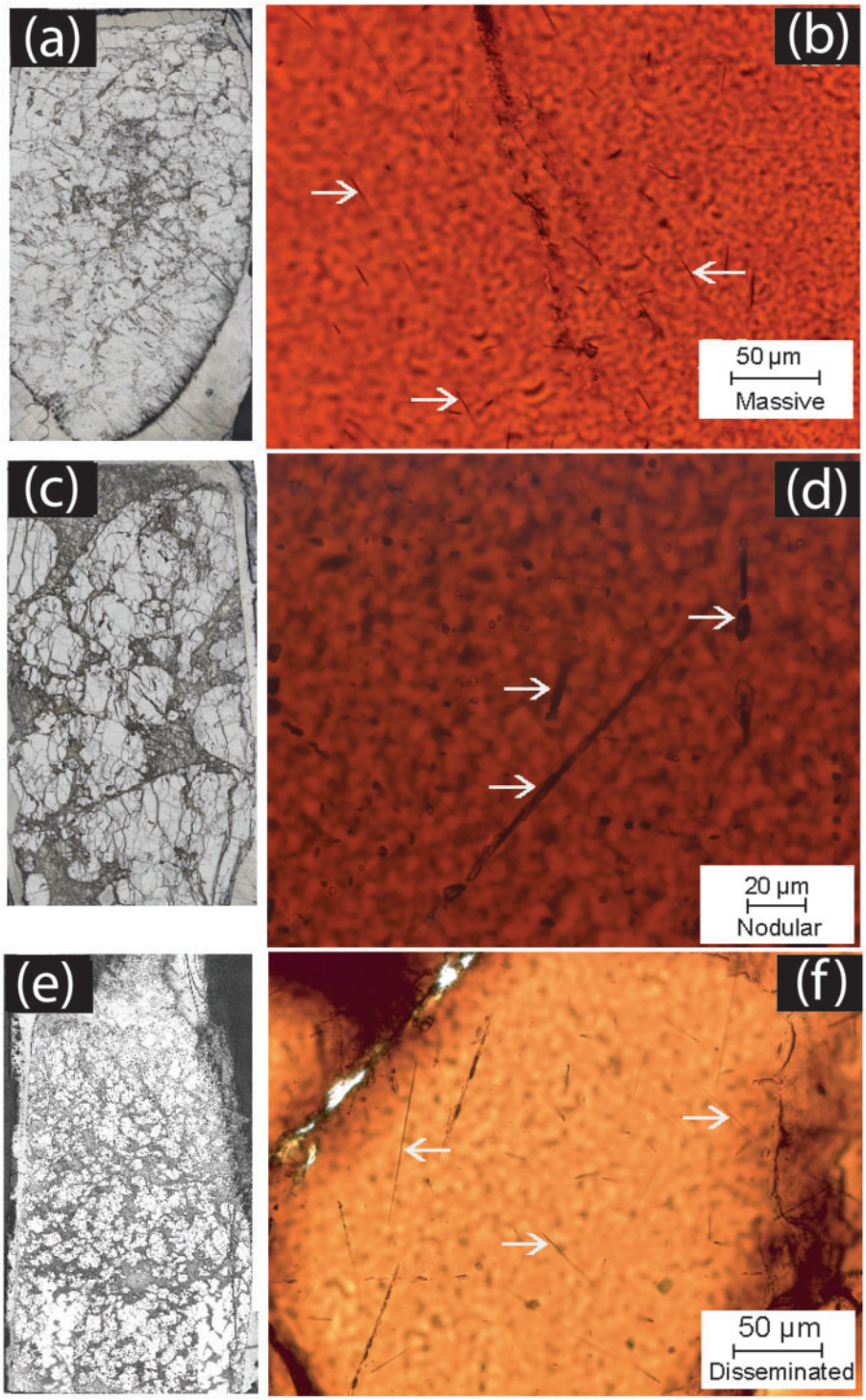

Fig. 3. Transmitted-light photomicrographs of chromite grains from massive (a, b), nodular (c, d) and disseminated (e, f) chromitites of the Luobusa and Kangjinla ore-bodies (arrows indicate exsolved needles and grains of diopside and SiO_2), accompanied by reflected light photomicrographs of the thin section of each sample (length of sections 3·5 cm).

We therefore suggest that phase BWJ formed through the subduction–dehydration of antigorite, equilibrating under conditions broadly consistent with the formation of ringwoodite or wadsleyite. The inverse-spinel structure is predicted to be stable at higher *T* but similar *P* (*c.* 2000°C at 15 GPa), compared with the normal ringwoodite structure (Kiefer *et al.*, 1999), although it does not appear to require the extreme conditions proposed by O'Neill & Navrotsky (1983). However, phase BWJ may have been stabilized at lower temperatures by the excess of Si, and the small contents of Al, Cr, Ni and Na (Table 3); experimental synthesis studies clearly are required.

Perhaps the single phase in these rocks that has aroused the most controversy is diamond; crystals

Table 2: *Major-element compositions (wt %) of clinopyroxene in WLG3-2 (massive chromitite), Luobusa*

	Euhedral separated $n = 16$ WDS	Exsolved *in situ* $n = 4$ EDS	Exsolved *in situ** $n = 1$ WDS
SiO_2	53·76	53·2	53·65
TiO_2	0·04	0·0	0·06
Al_2O_3	0·71	0·8	0·55
Cr_2O_3	0·59	2·3	2·56
FeO	1·08	1·4	1·03
MnO	<0·06		
MgO	18·31	17·6	18·97
NiO	0·08		
CaO	24·95	24·2	23·78
Na_2O	0·14	0·3	0·21
K_2O	0·00		
Total	99·64	100·0 (norm.)	100·81

*Needle of 5 μm × 50 μm.
WDS, wavelength-dispersive spectroscopy; EDS, energy-dispersive spectroscopy.

were recovered from heavy-mineral concentrates of the Luobusa chromitites more than 30 years ago (Bai *et al.*, 1993, 2001). Diamond was later reported from both chromitites and peridotites in several other massifs along the YZSZ (Fig. 1; Supplementary Data Table A1). These diamonds (typically 50–500 μm across; Fig. 6) are distinct from those found in kimberlites, including the 'superdeep' diamonds with inclusions of Transition Zone and lower mantle minerals. The diamonds from Luobusa have been briefly described in several papers (Robinson *et al.*, 2004; Yang *et al.*, 2007, 2014; Xu *et al.*, 2009, 2015) and characterized in detail by Howell *et al.* (2015). They display cubo-octahedral morphology with flat cubic faces, which are not found on kimberlitic diamonds, and imply growth in a metal solvent (i.e. melt; Howell *et al.*, 2015). The $\delta^{13}C$ of the diamonds studied by Howell *et al.* (2015) is unusually low (–24 to –29), especially when compared with cratonic diamonds; a wider range (–18 to –28) was reported by Xu *et al.* (2015). The diamonds have moderate contents of nitrogen (100–300 ppm), but with no evidence of aggregation to N_2 (C centres only; Type Ib). Their N-isotope compositions are highly unusual; $\delta^{15}N$ [determined by secondary ionization mass spectrometry (SIMS), University of Alberta] ranges from –5 to + 28, and varies by up to 20 within single stones, independently of the growth sectors. In contrast, HP–HT synthetic diamonds typically contain atmospheric N ($\delta^{15}N = 0$), and show a consistent difference of 30 between cubic and octahedral sectors. The $\delta^{15}N$ data for the Luobusa diamonds thus distinguish them from synthetic HP–HT diamonds, and also suggest disequilibrium crystallization.

The trace element patterns [analyzed by laser ablation inductively coupled plasma mass spectrometry (LA-ICP-MS)] of the Tibetan diamonds are broadly similar to those of kimberlitic diamonds, with overall light rare earth (LREE) enrichment. However, unlike kimberlitic diamonds, they also display marked negative

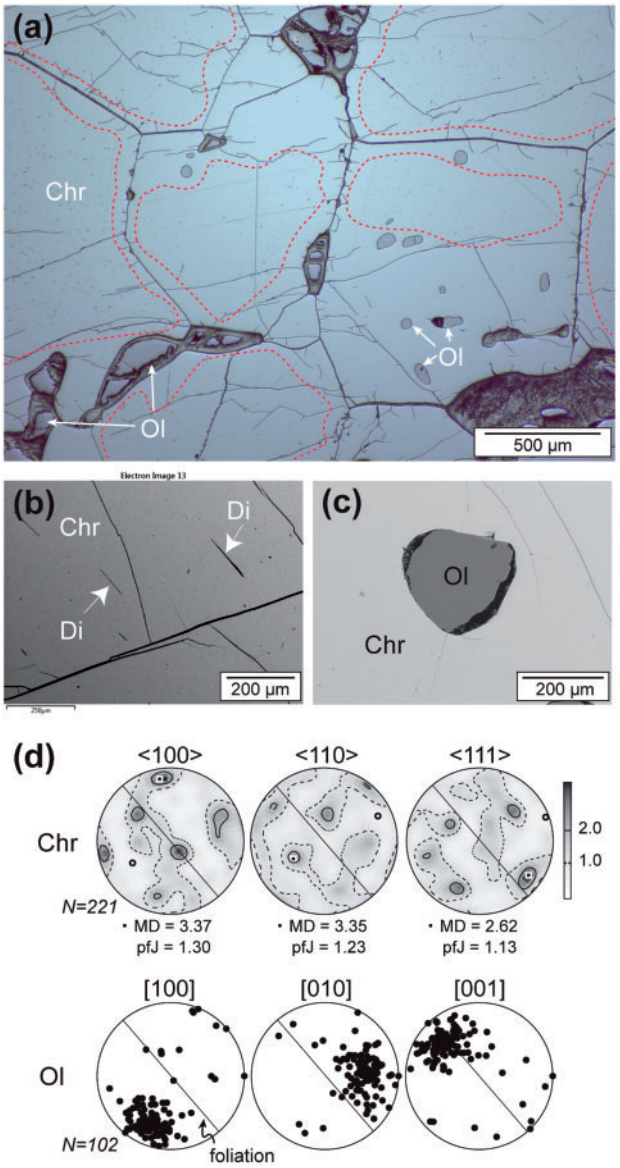

Fig. 4. (a) Photomicrograph showing equilibrated near-equigranular microstructure of massive chromitite, with exsolved diopside needles and a small included olivine (Ol) grain. Red dashed lines enclose areas with abundant exsolved needles of diopside and SiO_2. (b) Detail of chromite core, showing oriented needles of diopside (Di). (c) Detail of olivine inclusion in chromite. (d) CPOs of chromite (Chr) and olivine (Ol); lower hemisphere equal-area stereographic projections, after Satsukawa *et al.* (2015).

anomalies in redox-sensitive elements such as Eu, Sm, Yb and Y (Griffin *et al.*, 2013; Howell *et al.*, 2015), and Fe is essentially absent; these features link the diamonds to the SuR-UHP mineral assemblage. The most common inclusions in these diamonds are Ni–Mn–Co alloys (mean $Ni_{70}Mn_{25}Co_5$, but varying slightly in composition between localities); these appear from their shapes to have been trapped as melt droplets (Fig. 6c and d).

Many of the above characteristics (although not the highly variable $\delta^{15}N$), are similar to those of synthetic diamonds grown industrially in metal fluxes at high-*P*, high-*T* conditions. However, most synthetic diamonds

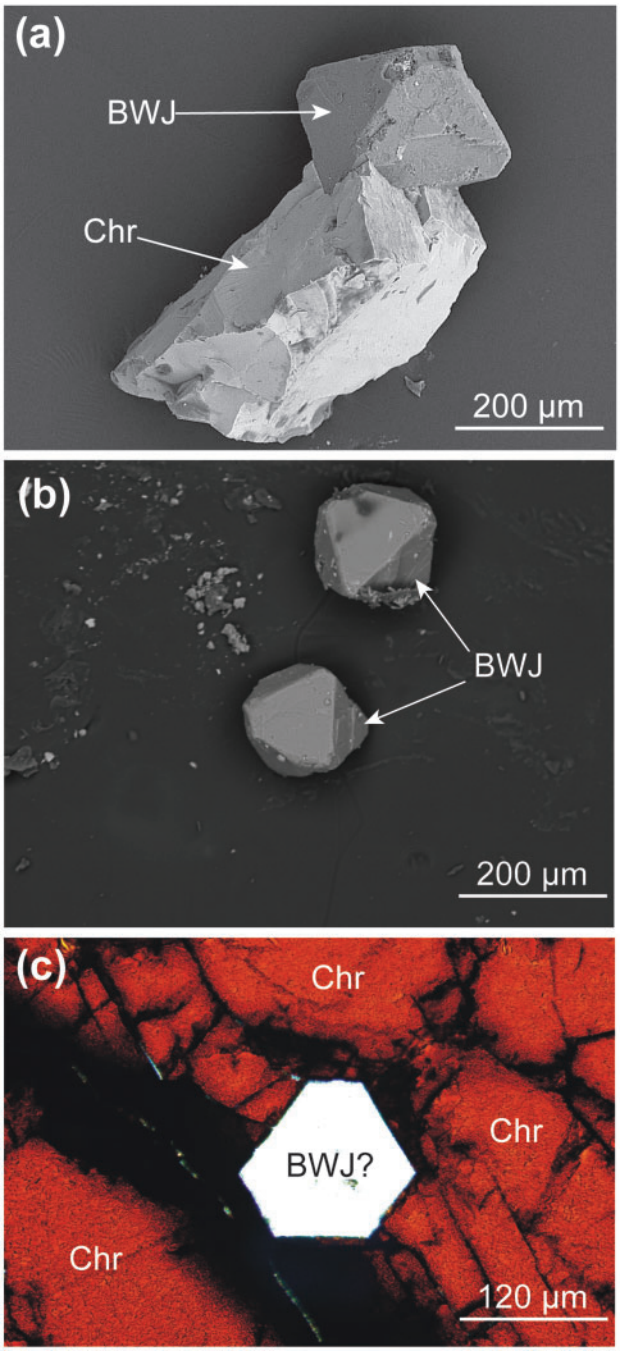

Fig. 5. Phase BWJ from the Luobusa chromitites. (a) SEM image of an octahedral BWJ crystal attached to chromite; (b) SEM image of separated octahedral, transparent BWJ crystals used for XRD studies; (c) transmitted-light photomicrograph of a possible pseudomorph after an octahedral crystal of BWJ, now altered to antigorite, enclosed in chromite. It should be noted that in these samples, olivine inclusions have rounded, rather than faceted shapes.

analyzed by us contain Fe (derived from the flux), which is essentially absent in the Tibetan diamonds owing to the low fO_2. We have recovered diamonds (40–250 μm; Fig. 6b) from single small (1–2 kg) samples, collected independently in the field and processed in a clean facility using selFrag techniques (electrostatic disaggregation; Teflon vessel; single-use disposable sieves), followed by hand-picking. This separation process is considered to rule out contamination by synthetic material.

Several diamonds have been observed *in situ* in polished sections (Yang *et al.*, 2007, 2014); they typically occur within spherical to amoeboid bodies of 'amorphous carbon' (the nature of which remains to be established) within chromite grains or breccia zones in chromitites. Single crystals of SiC and corundum have been reported in a similar microstructural setting (Xu *et al.*, 2015). The sum of evidence strongly suggests that the diamonds are natural, and represent a previously unrecognized process and environment for producing diamonds in the mantle. The diamond itself does not require Transition Zone (TZ) conditions to be stable, but the common $Ni_{70}Mn_{25}Co_5$ inclusions, which appear to have been trapped as melts, imply high T (>1200 °C; Gupta, 1999; see also SGTE alloy databases online), consistent with material originating in the deep upper mantle (see below).

Majoritic garnets in peridotites

One of the perplexing aspects of the Tibetan peridotites is the contradiction between the presence of UHP trace minerals (e.g. diamond) and the absence of garnet peridotites; all of the ultramafic rocks appear to have equilibrated at relatively shallow depths but high T (spinel- to plagioclase-peridotite facies; 0·5–1·5 GPa, 1100–1250°C; Hebert *et al.*, 2003; Liu *et al.*, 2010; Xiong, 2015). However, it was recently recognized that coarse symplectitic intergrowths of orthopyroxene + spinel ± clinopyroxene (Fig. 7) may represent the breakdown products of high-pressure majoritic garnet. These have been identified in the Purang peridotite (Gong *et al.*, in preparation) and have previously been described from other diamond-bearing peridotites along the YZSZ (Fig. 1; Xigaze, Hebert *et al.*, 2003; Zedang, Xiong, 2015). They are similar in appearance and occurrence to other pyroxene + spinel intergrowths interpreted as relics after mantle garnet: in peridotite xenoliths in kimberlites (Haggerty & Sautter, 1990; Sautter *et al.*, 1991; Field & Haggerty, 1994; Medaris *et al.*, 1997) and basalts (Smith, 1997; Shimizu *et al.*, 2008), in crustal UHP peridotites (Horoman complex, Morishita & Arai, 2003), and in peridotite massifs showing other evidence for a deep origin (Lanzo, Piccardo *et al.*, 2007; Ronda, Tubía *et al.*, 2004).

Reconstruction of the garnet compositions, following the procedures recommended by Takahashi (2001) and Morishita & Arai (2003) (Supplementary Data Table A3) gives Si contents (relative to 12 oxygens and eight cations) of 3·2–3·6, implying pressures >13 GPa (>400 km), well within the Transition Zone [see Griffin (2008) and Corgne *et al.* (2012) for summaries of relevant experimental work]. The high Cr content of the spinels, and of the reconstructed garnets, effectively rules out alternative origins, such as exsolution from high-T, low-P orthopyroxene. Interestingly, many of these same

Table 3: *Comparison of major-element analyses (wt %) of phase BWJ and antigorite*

Mineral:	Phase BWJ		Brown octahedra			Antigorite	
Type:	Inverse spinel		Antigorite			Antigorite	
Locality:	Luobusa		Luobusa, Kangjinla			Rock Springs, USA	
	Range ($n = 4$)	Mean	Range ($n = 6$)	Mean	Norm	$n = 1$	Norm
SiO_2	49·6–50·9	50·5	42·4–43·1	42·9	50·0	44·5	50·6
TiO_2	0·00–0·05	0·02	0–0·01	0	0·00		
Al_2O_3	0·80–1·07	0·91	0·29–0·74	0·47	0·55	1·4	1·6
Cr_2O_3	0·54–0·0·64	0·59	0·20–0·56	0·35	0·41	0·06	0·07
FeO	1·21–1·44	1·30	0·91–1·2	0·98	1·14	0·35	0·40
NiO	0·17–0·22	0·18	0·12–0·27	0·17	0·20	0·1	0·11
ZnO	0·02–0·12	0·05		0·00	0·00		
MnO		0·00		0·00	0·00		
MgO	46·1–47·8	47·1	40·2–41·2	40·9	47·6	41·6	47·2
CaO	0·04–0·08	0·05	0·03–0·08	0·04	0·05		
Na_2O	0·08–0·19	0·12	0·004–0·02	0·01	0·01		
K_2O	0·08–0·11	0·09	0·007–0·013	0·01	0·01		
H_2O						12·4	
Total	99·9–102·0	100·94	85·0–86·8	85·8	100	100·18	100

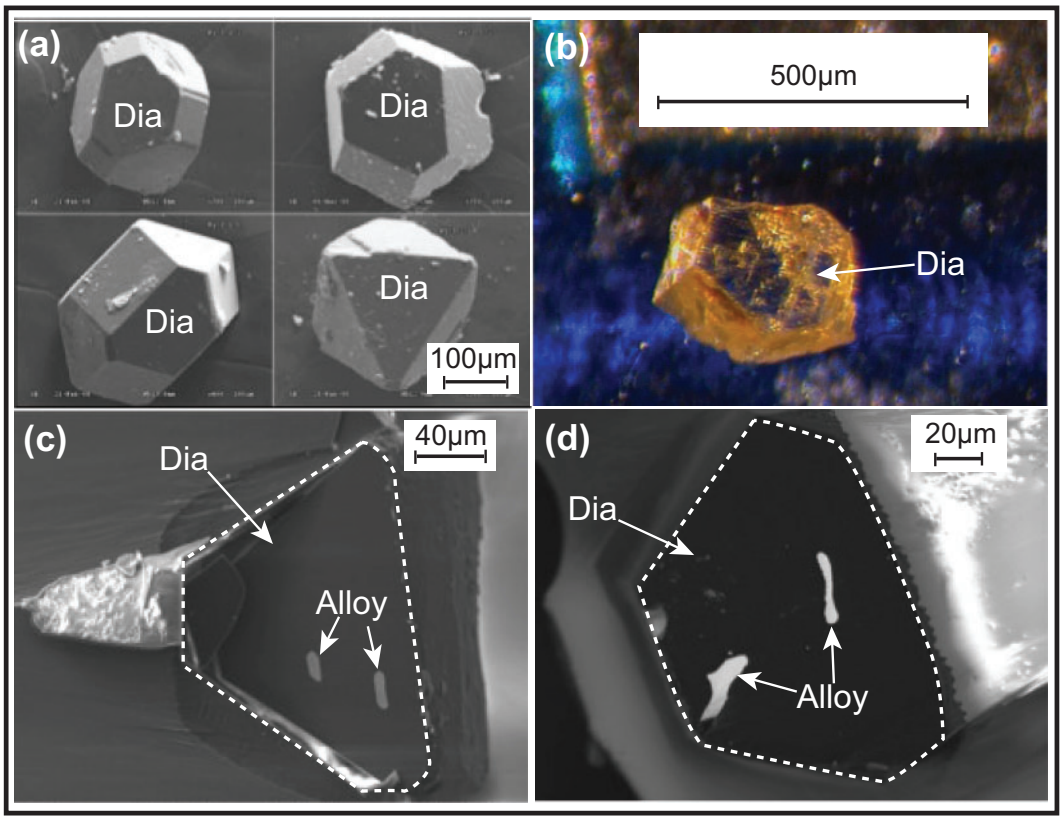

Fig. 6. Diamonds (Dia) from Luobusa chromitites. (a) BSE images, showing cubo-octahedral morphology; (b) binocular microscope image of diamond separated in the laboratories of the ARC Centre of Excellence for Core to Crust Fluid Systems (Macquarie University) from an independently collected chromitite sample from Luobusa; (c, d) BSE images of metallic inclusions ($Ni_{70}Mn_{20}Co_5$) exposed by Ar-ion milling of diamond crystals (outlined by white dashed lines).

peridotites do contain large orthopyroxene porphyroblasts with several generations of finely lamellar exsolution of cpx and Al-spinel, suggesting rapid cooling from high *T* (Hebert *et al.*, 2003; Xiong, 2015).

Evidence for a shallow beginning

If the chromitites and the peridotites in at least some of the massifs of the YZSZ have come from the deep upper mantle or Transition Zone, how did they get there in the first place? Do they represent the primary composition of this deep mantle, or parts of shallower mantle subducted to Transition Zone depths? The compositions of the peridotites, both depleted and fertile, have their counterparts in the mantle sections of other ophiolitic complexes worldwide; the most depleted peridotites are usually found in ophiolites

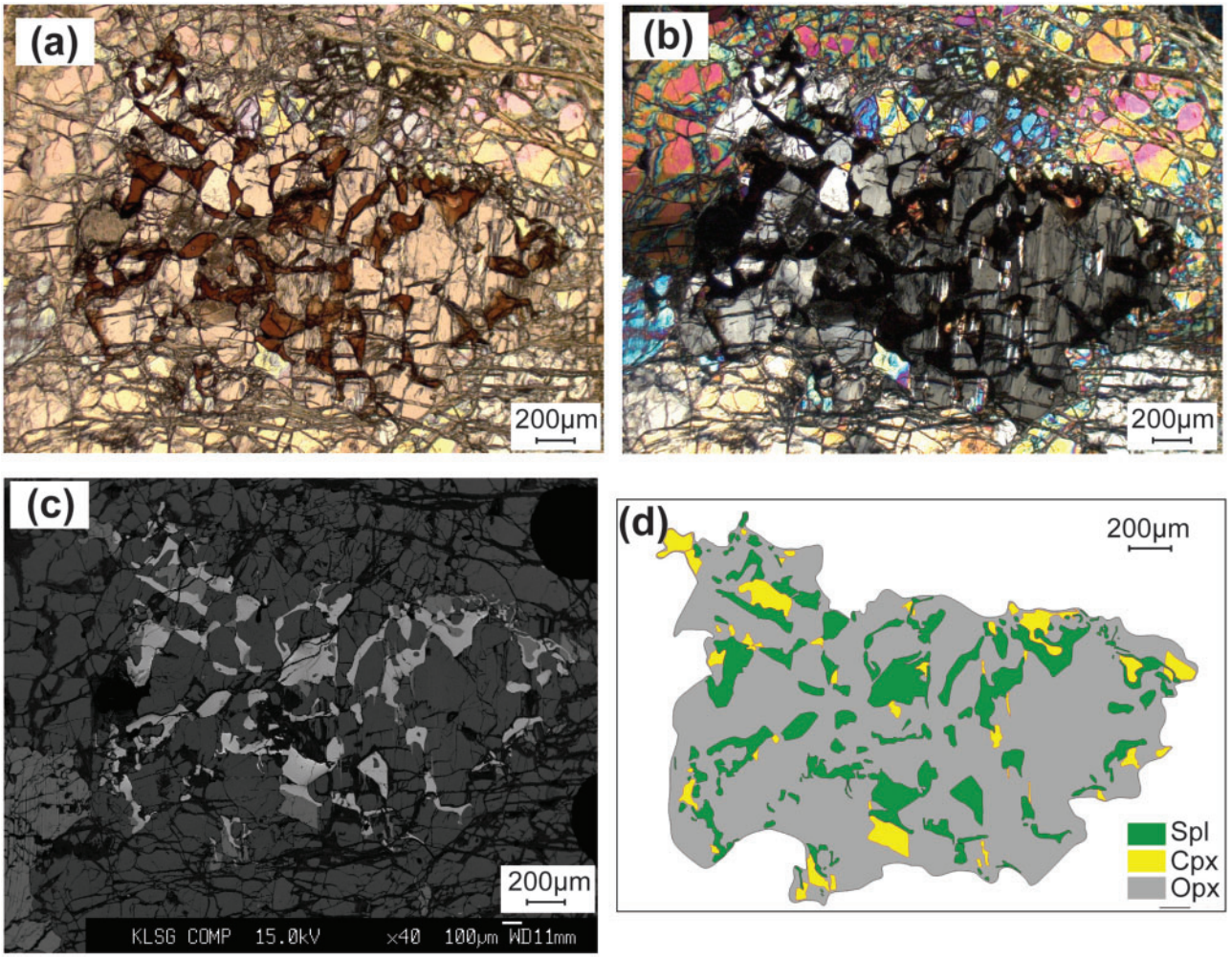

Fig. 7. Coarse symplectite of Cr–Al spinel and orthopyroxene, interpreted as a breakdown product of majoritic garnet. (a) Plane-polarized and (b) crossed-polarized photomicrographs; (c) BSE image; spinel shows as bright areas, pyroxenes as dark areas; (d) phase map used for reconstruction as discussed in the text. The original garnet, reconstructed following the olivine subtraction approach of Takahashi (2001) has the composition SiO_2 49·2%, Al_2O_3 13·6%, Cr_2O_3 6·9%, FeO 7·3%, MgO 24·4%, CaO 2·4%, and minor Ti and Mn; this gives Si 3·23 atoms for eight cations and 12 oxygens, corresponding to a pressure of *c.* 13·5 GPa (Corgne *et al.*, 2012).

from SSZ environments, whereas the less depleted types may occur in several types of tectonic setting (Dilek & Furness, 2011). There are no known processes that would produce the depleted peridotite compositions within the Transition Zone, because high degrees of partial melting are restricted to the uppermost 150–200 km of the mantle (Green & Falloon, 1998). This suggests that these peridotites were originally carried into the Transition Zone from shallower environments.

The new cubic Mg-silicate (phase BWJ) described here is the anhydrous compositional analogue of antigorite; this is consistent with an origin as antigorite, trapped within chromite grains at shallow levels. We suggest that thin serpentine veinlets were necked down and annealed into inclusions with negative crystal forms, analogous to the development of fluid inclusions from fluid-filled cracks. Serpentine minerals break down at depths of 220 km or less in subduction zones (Ulmer & Trommsdorff, 1995), to be succeeded with increasing pressure by a series of dense hydrous magnesium silicates (e.g. Kawamoto, 2004; Litasov & Ohtani, 2007). We therefore interpret the presence of phase BWJ as evidence that the enclosing chromitites originated at shallow levels and low *T*, where they could be serpentinized, and then were dehydrated during subduction, and/or by heating during residence of the subducted material in the Transition Zone.

This suggestion is consistent with the major and trace element signatures of the YZSZ chromitites themselves. They are typical of SSZ chromitites in ophiolitic complexes that show no evidence of subduction (González-Jiménez *et al.*, 2014*b*; McGowan *et al.*, 2015). Indeed, a major element geochemical study of the chromitites of the Luobusa massif, where evidence of Transition Zone metamorphism is most abundant, concluded that the chromitites crystallized from 'boninitic melts' (Zhou et al., 1996, 2014); in other words, they originated in a relatively shallow SSZ environment.

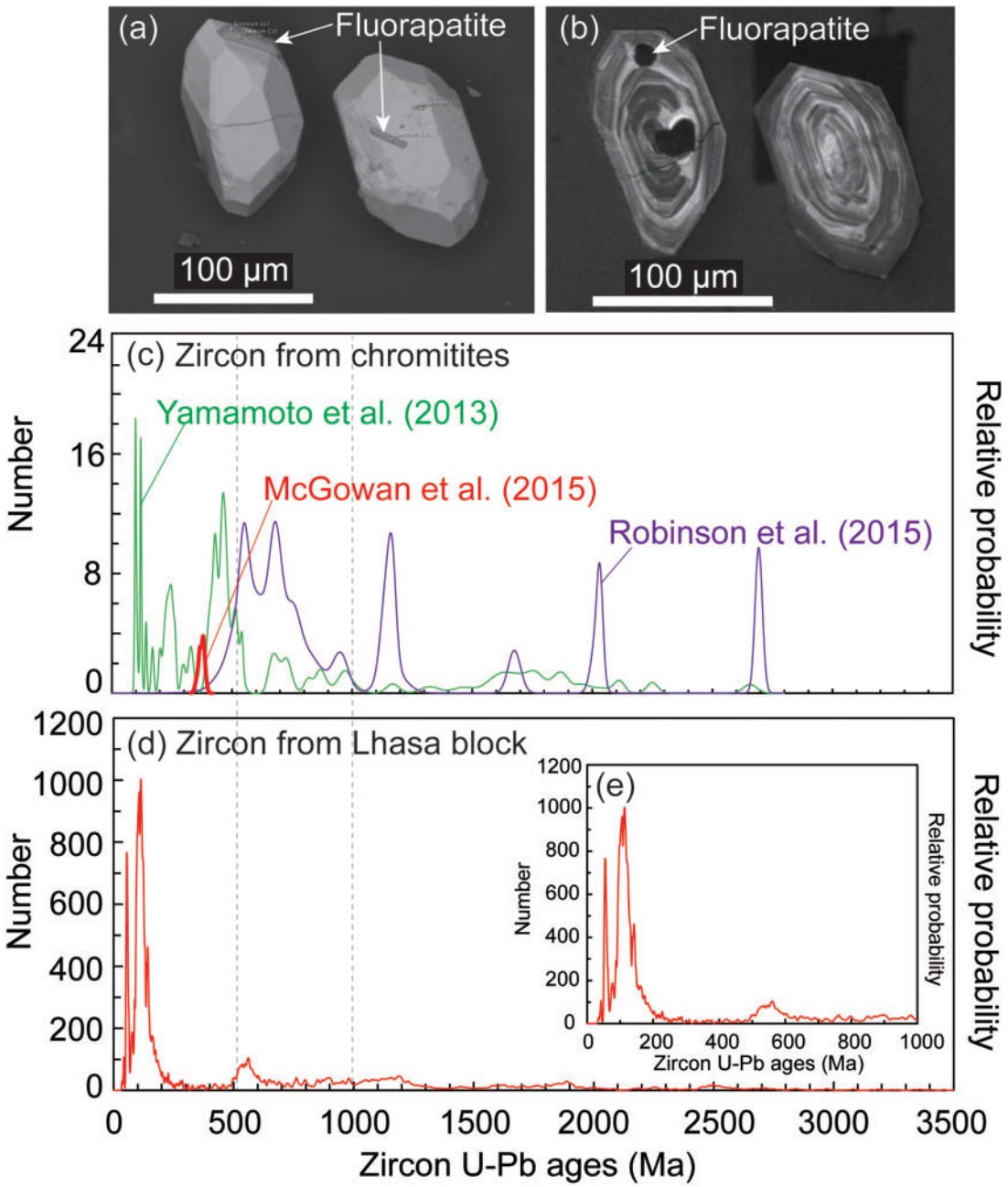

Fig. 8. (a, b) Magmatic zircons (note fluorapatite prisms on surfaces, and as inclusions in the zircons with oscillatory zoning) separated from Luobusa chromitite [(a) secondary electron image; (b) cathodoluminescence image]; (c) ages of zircons from the Luobusa chromitites, with references; (d, e) ages of zircons from plutonic rocks of the Lhasa block (Leier *et al.*, 2007), and detrital zircons from the Lhasa block (Wu *et al.*, 2010; Aitchison *et al.*, 2011). A noteworthy feature is the presence in both (c) and (d, e) of the major peaks at *c.* 120 Ma, extending to ages (<100 Ma) significantly younger than the age of ophiolite emplacement (*c.* 130 Ma), and a major population between 400 and 1000 Ma, as well as a scatter of older inherited grains.

A second line of evidence comes from magmatic zircons found in some of the chromitites. Previous, large-scale sampling of the chromitites has yielded abundant zircons, but those that have been described (Yamamoto *et al.*, 2013; Robinson *et al.*, 2015) clearly are xenocrystic. Their morphologies suggest a detrital history; they contain abundant inclusions of crustal minerals and they show a range of concordant ages from Archean to 96 Ma, the latter significantly younger than the final accretion age (*c.* 130–120 Ma) of the ophiolites. We also have separated such zircons from hand-samples, but regard them as irrelevant to the origins of the ophiolitic peridotites (see discussion below).

However, some samples of massive chromitite contain a single, well-defined population of euhedral, obviously magmatic zircon (Fig. 8; McGowan *et al.*, 2015) with O- and Hf-isotope compositions indicative of mixing between mantle-derived and slab-derived melts. Such mixing or mingling of melts is also the most probable mechanism for the generation of chromitites in

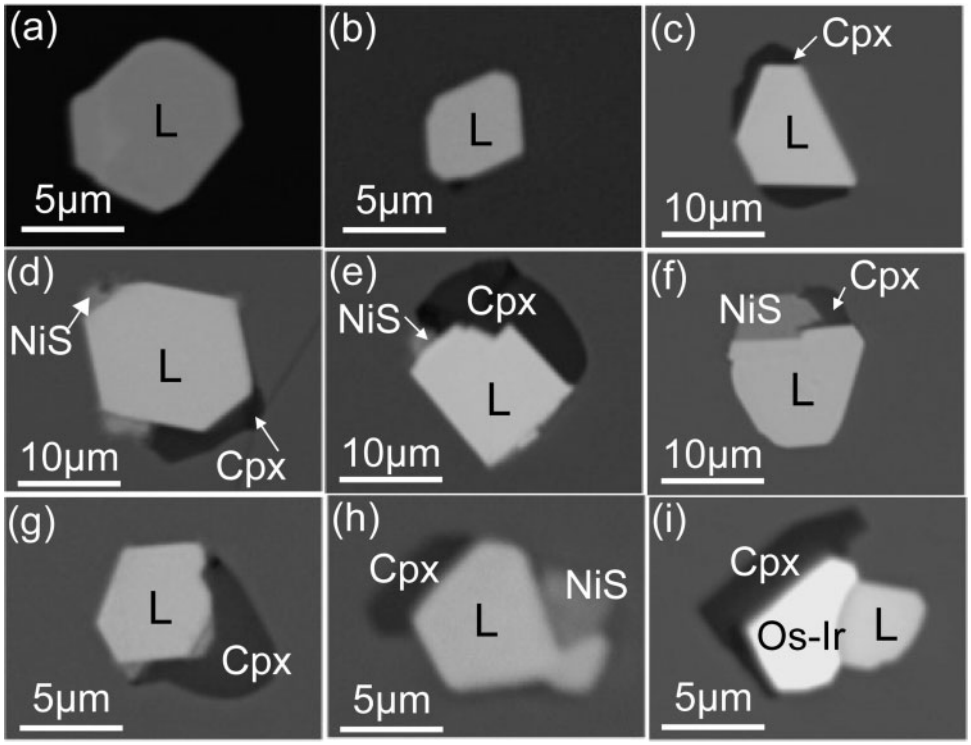

Fig. 9. Platinum-group minerals and NiS enclosed in chromitite from Kangjinla; the nucleation of exsolved clinopyroxene on PGM, and the negative crystal morphology of the PGM and attached silicate phases, should be noted. L, laurite; Os–Ir, Os–Ir alloy; Cpx, clinopyroxene.

SSZ environments (see review by González-Jiménez *et al.*, 2014b). This population gives a well-defined Concordia age of 376 ± 7 Ma.

The same samples, and others examined by us, contain inclusions of laurite (RuS_2) and rare Os–Ir, typical of many SSZ chromitites (Fig. 9; González-Jiménez *et al.*, 2014a); we interpret these as primary magmatic phases. *In situ* analysis of their Os-isotope compositions (Table 4) gives T_{RD} ages ranging mainly from *c.* 100 to 630 Ma with a pronounced peak at *c.* 340 Ma (Fig. 10a); this peak is within the uncertainties of the zircon age, and both ages are significantly older than the emplacement of the peridotites to shallow levels (*c.* 170–150 Ma; see below). The platinum-group minerals (PGM) occur in chromites showing the cpx–SiO_2 exsolution, described above, and have served as nucleation points for the exsolution of diopside and possibly olivine (Fig. 9). We suggest that these are SSZ PGM, formed as liquidus phases and trapped during the precipitation of the chromite (see Brenan & Andrews, 2001; Bockrath *et al.*, 2004). This implies that they survived subduction into the Transition Zone and the conversion of the chromite to the CF-structured polymorph. Such survival appears to be inconsistent with experiments showing that laurite is replaced by Ru–(Os–Ir) alloys with increasing T >1275°C (Brenan & Andrews, 2001). However, these were 1 atm experiments and the pressure effect is unknown; the apparent coexistence of laurite and Os–Ir (Fig. 9i) may document a two-phase stability field at higher pressures and temperatures.

A suggested *P–T–t* path

A *P–T* grid constructed from published experimental work, the reported mineralogy and available geochronology suggests a *P–T–t* path for the Luobusa–Kangjinla massif and some other YZSZ peridotites (Fig. 11a). The antigorite stability field is taken as the starting point, based on the proposed original composition of phase BWJ from Luobusa, and other evidence of a shallow origin. The curve defining the breakdown of diopside to olivine (wadsleyite–ringwoodite) + $CaSiO_3$ perovskite + stishovite probably represents a maximum depth, as euhedral diopside, clearly in textural and chemical equilibrium with chromite (Table 2; Fig. 3), is abundant in some samples, but Ca-perovskite has not been recognized. The work of Satsukawa *et al.* (2015) implies *P–T* conditions in the stability field of wadsleyite, which may also be consistent with the presence of the inverse-ringwoodite structure of phase BWJ, as discussed above.

The significance of the exsolution of coesite and chromite was recognized by Arai (2010, 2013), who suggested a recycling process, although without other constraints or a proposed mechanism. The conversion of chromite to the CF structure was originally studied by Chen *et al.* (2003), who determined a pressure of 12·5 GPa at 2000°C. This pressure was later taken as the depth of the transition in the Luobusa chromitites (Yamamoto *et al.*, 2009; Yang *et al.*, 2015), without considering the possible temperature dependence. More recent work suggests pressures >24 GPa at 300 K (Kyono *et al.*, 2009) and studies using natural Luobusa

Table 4: In situ *Re–Os isotopic compositions of laurite from chromitites in the Luobusa ophiolite, south Tibet*

Sample ID	$^{187}Re/^{188}Os$	1σ	$^{187}Os/^{188}Os$	1σ	T_{RD} (Ga)_ECR	1σ (Ga)	Data sources
SRL-1A-P2	–0·00056	0·00012	0·12524	0·00003	0·406	0·004	This study
LBS14-6G-P2	–0·00020	0·00030	0·12512	0·00084	0·424	0·119	This study
LBS14-7B-P2	–0·00020	0·00030	0·12512	0·00084	0·424	0·119	This study
LBS14-7E-P1	0·00008	0·00006	0·12593	0·00015	0·309	0·021	This study
LBS14-7P-P2	0·00041	0·00047	0·12638	0·00034	0·245	0·048	This study
LBS14-8J-P1	0·00007	0·00004	0·12571	0·00003	0·340	0·004	This study
LBS14-8G-P1	0·00056	0·00017	0·12589	0·00030	0·315	0·043	This study
LBS14-5E-P1	0·00006	0·00008	0·12615	0·00020	0·277	0·028	This study
LBS14-5D-P1	0·00014	0·00007	0·12573	0·00010	0·337	0·014	This study
LBS14-6D-P1	0·00004	0·00030	0·12612	0·00016	0·281	0·023	This study
KJL14-9D-P2	0·00060	0·00053	0·12267	0·00060	0·770	0·084	This study
LBS14-6G-P1	–0·00014	0·00010	0·12697	0·00012	0·160	0·017	This study
KJL14-2FK4	0·00066	0·00009	0·12713	0·00020	0·139	0·028	This study
LBS14-8D-P2	0·00000	0·00036	0·12755	0·00052	0·078	0·074	This study
LBS14-5F-P1	0·00014	0·00013	0·12776	0·00028	0·048	0·040	This study
LA-623B-2-PTO1	0·00001	0·00026	0·12583	0·00029	0·322	0·041	McGowan et al., 2015
LA-623B-2-PTO2	0·00002	0·00010	0·12509	0·00045	0·428	0·064	McGowan et al., 2015
LA-623B-2-PTO3a	0·00000	0·00008	0·12588	0·00016	0·316	0·023	McGowan et al., 2015
LA-623B-2-PTO3	0·00004	0·00006	0·12611	0·00012	0·283	0·017	McGowan et al., 2015
LA-586B-1-PTO1	0·00003	0·00002	0·12567	0·00015	0·345	0·021	McGowan et al., 2015
LA-586B-1-PTO2	0·00033	0·00031	0·12609	0·00039	0·286	0·055	McGowan et al., 2015
LA-623B-PTO1	0·00125	0·00046	0·12561	0·00050	0·354	0·071	McGowan et al., 2015
LA-623B-3-PTO4	0·00014	0·00009	0·12515	0·00030	0·419	0·042	McGowan et al., 2015
LA-623B-1-PTO3	0·00007	0·00007	0·11449	0·00009	1·909	0·013	McGowan et al., 2015
LA-623B-3-PTO2b	0·00003	0·00003	0·12368	0·00006	0·626	0·008	McGowan et al., 2015
LA-623B-3-PTO2a	0·00028	0·00025	0·12382	0·00027	0·607	0·038	McGowan et al., 2015
LA-586A-1-PTO1a	0·00084	0·00012	0·12421	0·00017	0·553	0·024	McGowan et al., 2015
LA-623B-1-PTO2	0·00004	0·00004	0·12436	0·00007	0·531	0·010	McGowan et al., 2015

T_{RD}, Re-depleted model ages calculated following Shirey & Walker (1998); model ages are based on the enstatite chondrite reservoir (ECR; Walker et al., 2002). Analyses by LA-MC-ICP-MS following techniques outlined by Shi et al. (2007).

chromitite as a starting material have determined pressures close to 14 GPa at 1600°C (Wu *et al.*, 2011; Jin *et al.*, 2014). The curve in Fig. 11 has been provisionally drawn on the basis of these data; it appears to agree with other indications and to support a pressure range in the upper part of the Transition Zone.

We therefore suggest that the subducted SSZ mantle arrived in the upper Transition Zone (13·5–15 GPa) at temperatures of the order of 850–1100 °C, consistent with numerous models of slab geotherms (Fig. 11b). During residence in the upper part of the Transition Zone, it may have been heated to temperatures ≥1500°C. Constraints on the degree of heating may be provided by some of the trace minerals. Separates from the chromitites and peridotites contain abundant spherules of Fe, typically rimmed by FeO and with inclusions of various Fe–Ti alloys (Fig. 2; Robinson *et al.*, 2004; Xu *et al.*, 2015). If these formed as melts, the implied temperatures are >1500°C (Fig. 11b). A minimum *T* may be derived from the melting *T* at $P = 14$ GPa (1300–1350°C; Gupta, 1999) of the Ni–Mn–Co alloys included in the diamonds.

We therefore illustrate two adiabatic exhumation paths beginning in the Transition Zone, one starting at ≥1500°C and the other at *c.* 1300°C (Fig. 11b, point 1). In this scheme, the diamonds could in principle form anywhere from the Transition Zone to the depth of the diamond–graphite reaction. The time–temperature requirements imposed by the N-aggregation data (Howell *et al.*, 2015) suggest that the shallower depths and lower temperatures (point 2) may be more probable (see below), but do not explain the apparent presence of Fe melts. Both paths are curved at shallow depth, reflecting rapid cooling relative to uplift, to avoid crossing the dry harzburgite solidus, as there is no field evidence for melting of the peridotites. Each of these paths cools through the last equilibration conditions defined for the spinel peridotites (Point 3; 1155–1255°C, 0·5–1·1 GPa; Girardeau & Mercier, 1988) and the *P–T* estimates from garnet–clinopyroxene amphibolites interpreted as the emplacement soles of the peridotite massifs (Point 4; 750–875°C, 1·3–1·5 GPa at *c.* 125 Ma; Guilmette *et al.*, 2008).

Summary of timing of events

There are several time constraints on the *P–T–t* path, as follows. (1) Generation of the chromitites in an SSZ environment at *c.* 375 Ma (McGowan *et al.*, 2015; Fig. 8c); subduction may have followed within 10–40 Myr, the typical life of such systems (Dai *et al.*, 2012). Similar ages (364–373 Ma) have been reported for gabbros from the Dangxiong and Najiu ophiolites (Dai *et al.*, 2011), and from the Iranian sector of the extended suture (Moghadam *et al.*, 2015), and have been taken as evidence of a relationship to subduction within the Paleo-Tethys ocean. (2) Residence in the Transition Zone until at least 230 Ma, as defined by the Re–Os T_{DM} ages of Os–Ir nuggets from Luobusa, with compositions indicating high *T* (Fig. 10b; Shi *et al.*, 2007). (3) Stratigraphic evidence (deposition of marine sediments

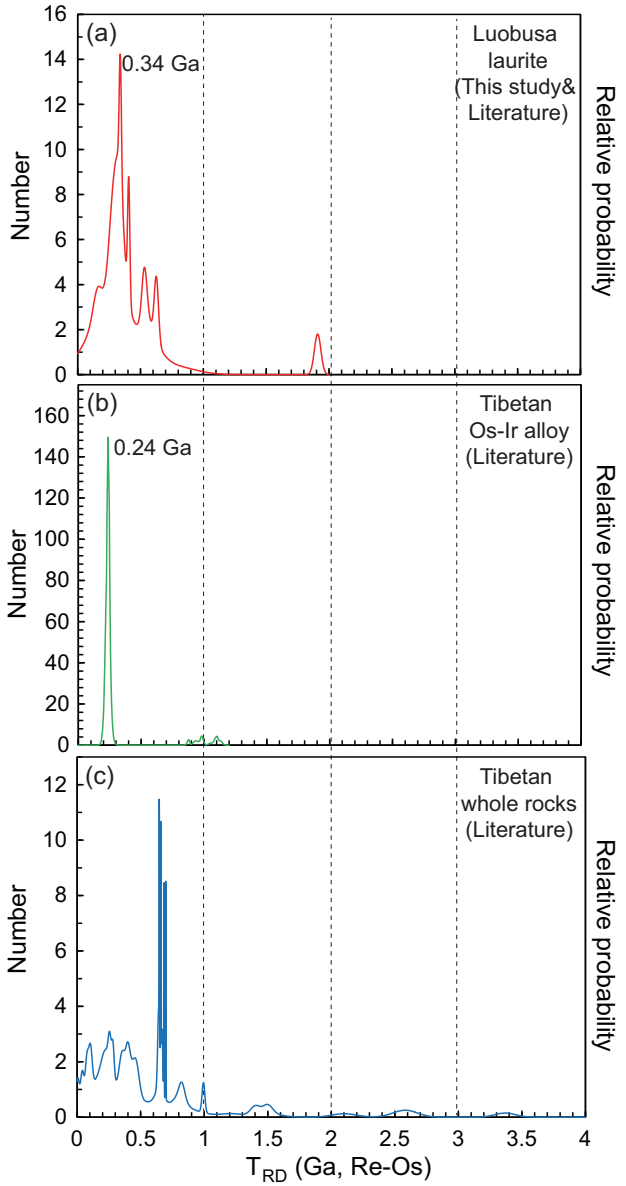

Fig. 10. Histograms of rhenium-depletion model ages (T_{RD}) for (a) laurite grains enclosed in chromitite from Luobusa, analyzed *in situ* in polished sections (data from Table 4); (b) large Os–Ir nuggets separated from chromitites of the Luobusa and Dongqiao peridotites (*in situ* analyses; data from Supplementary Data Table A4), and (c) whole-rock samples of chromitites and peridotites from the YZSZ (data from Supplementary Data Table A4). Vertical dashed lines mark model ages of 1, 2 and 3 Ga.

directly on the peridotites), and dating of dikes that cross-cut serpentinized peridotites, suggests that some massifs were emplaced to very shallow depths, probably at the sea floor (see below), by late Jurassic times (*c.* 150–170 Ma) whereas others were emplaced over a short period around 120–135 Ma (Girardeau *et al.*, 1985*a*, 1985*b*; Dai *et al.*, 2013; Liu *et al.*, 2014; Xiong *et al.*, 2016). Thus the Luobusa peridotite may have spent at least *c.* 200 Myr in the Transition Zone before being exhumed.

DISCUSSION

An evolutionary model

Putting the evidence presented here into a geodynamic context requires plausible answers to the following two questions. (1) How did the SSZ mantle peridotites containing the chromitites reach TZ depths? (2) How did they come back to shallow depths?

In light of our current understanding of geodynamic processes in collisional environments, the second question is easier to answer. Moresi *et al.* (2014) have modeled the process of slab roll-back and the accumulation of subducted material in the Transition Zone, and shown how an impediment to subduction in one segment of a suture (for example, by the arrival of a sliver of continental material) leads to accelerated roll-back in adjacent segments. This tectonic situation is typical of the late-stage closure of ocean basins, especially near the tips of 'ribbon continents' such as those that make up the Tibetan margin. Such roll-back induces large-scale mantle upwelling in front of the retreating slab.

Afonso & Zlotnik (2011) used two-dimensional thermomechanical simulations to model the evolution of a collisional zone that experiences such slab roll-back. The results of such modeling show that passive upwelling (forced return flow) begins as a large-scale, long-wavelength feature in response to both the downward penetration of the slab into the mantle and its roll-back, but quickly develops into a narrow upwelling rising rapidly from the Transition Zone (McGowan *et al.*, 2015; Fig. 12). This narrow upwelling channel is favored by non-linear rheologies (Afonso & Zlotnik, 2011). Although the upper mantle involved in the upwelling will experience large shear strains, harzburgitic bodies embedded within the upwelling mantle will undergo significantly less internal deformation. This is due to the rheological (i.e. viscosity) contrast expected between the normal (water-rich) mantle and the much drier harzburgite volumes (see Manga, 1996; Karato, 2008). Typically, dehydration owing to partial melting increases viscosity by factors of 50–100 in olivine-rich rocks (e.g. Afonso *et al.*, 2008; Karato, 2008), and even a factor as low as 10 will effectively isolate the higher-viscosity volumes from significant strain during upwelling (Manga, 1996). As noted above, many of the YZSZ peridotites appear to be unusually anhydrous except in zones of obvious later tectonism associated with their crustal history. The exhumation process would be even more effective if the material in the Transition Zone was inherently buoyant, as in the case of thermally equilibrated, depleted harzburgite. A harzburgitic body could retain up to ~5% chromitite and still remain buoyant; the geological map of the Luobusa massif, which contains the largest and most abundant chromitite deposits, suggests that the actual proportion of chromitite is $< 1\%$.

The numerical simulations of Afonso & Zlotnik (2011) and Moresi *et al.* (2014) suggest that the time scale for transport of a large body of harzburgite from

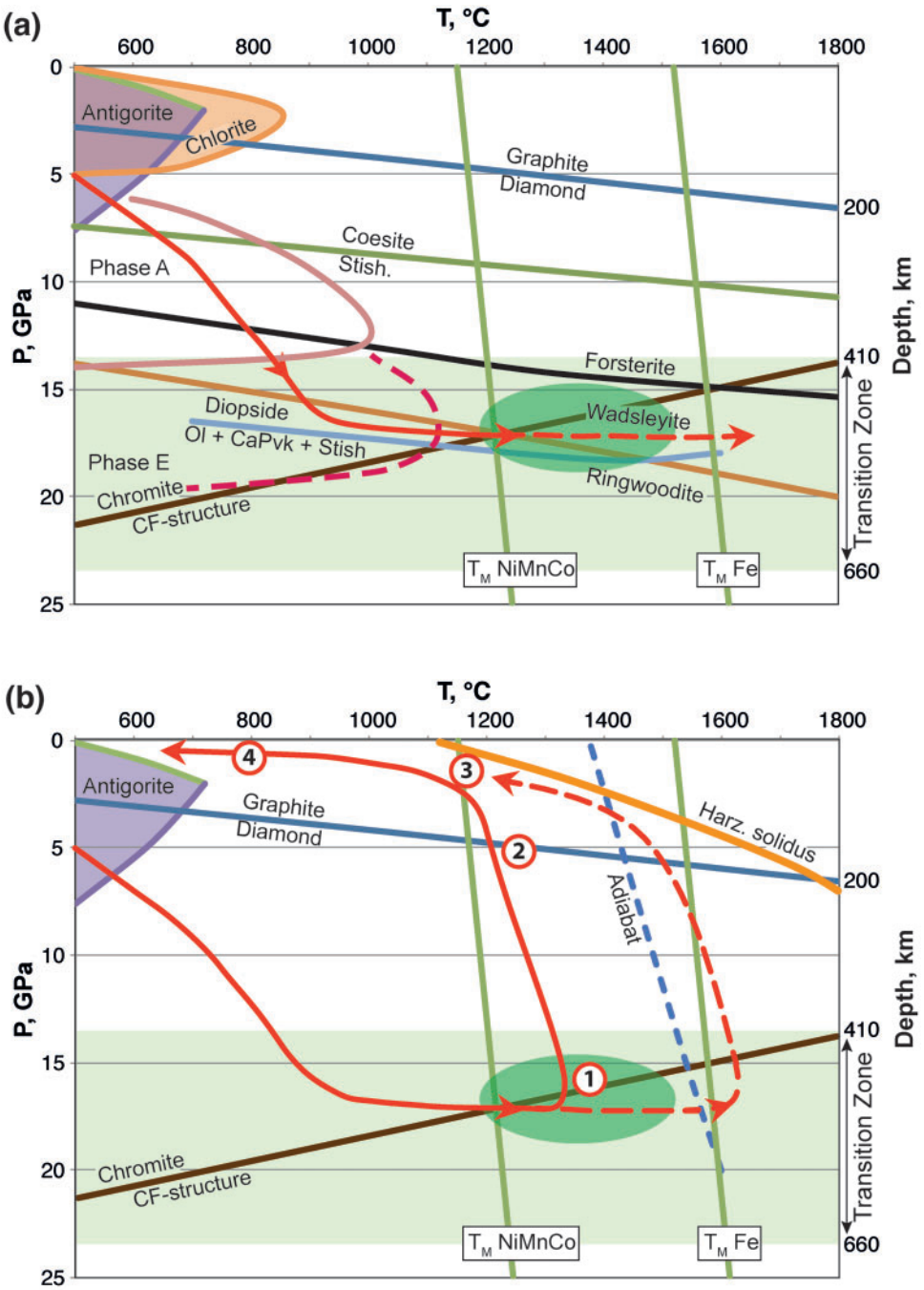

Fig. 11. Reconstructed *P–T–t* path for the Luobusa–Kangjinla peridotite body. (a) Stability fields of hydrous phases and curves for relevant reactions and *T* constraints (for data sources see text); green oval indicates a probable *P–T* region for coexistence of wadsleyite, CF-structured chromite and majoritic garnet. Red arrow illustrates subduction of mantle wedge material into the Transition Zone, followed by heating to at least 1300 °C, the melting point of alloy inclusions in diamonds (T_M NiMnCo; Fig. 6) at TZ depths, or to > 1500 °C [melting point of Fe (T_M Fe; Fig. 2)]. (b) Two end-member (low-*T*, high-*T*) uplift paths (red continuous and dashed curves with arrow), parallel to the mantle adiabat, are illustrated. Formation of diamonds is possible at point (1), but formation near point (2) would be more consistent with the lack of nitrogen aggregation in the diamonds. Points (3) and (4) represent points on the path determined by geothermobarometry (see text).

~500 km depth to shallow lithospheric levels by the above process is of the order of 7–10 Myr. The last 100 km of the ascent would take significantly less than 1 Myr, and would be followed by rapid cooling at shallow depths. This model has several attractive features, including a plausible mechanism for the preservation of diamonds with unaggregated nitrogen in both harzburgites and chromitites (Howell *et al.*, 2015), coesite inclusions in chromitites (Yamamoto *et al.*, 2009), and oriented needles of diopside and magnetite in the olivine of dunites (Ren *et al.*, 2008). The prismatic aggregates of coesite/stishovite and kyanite described by

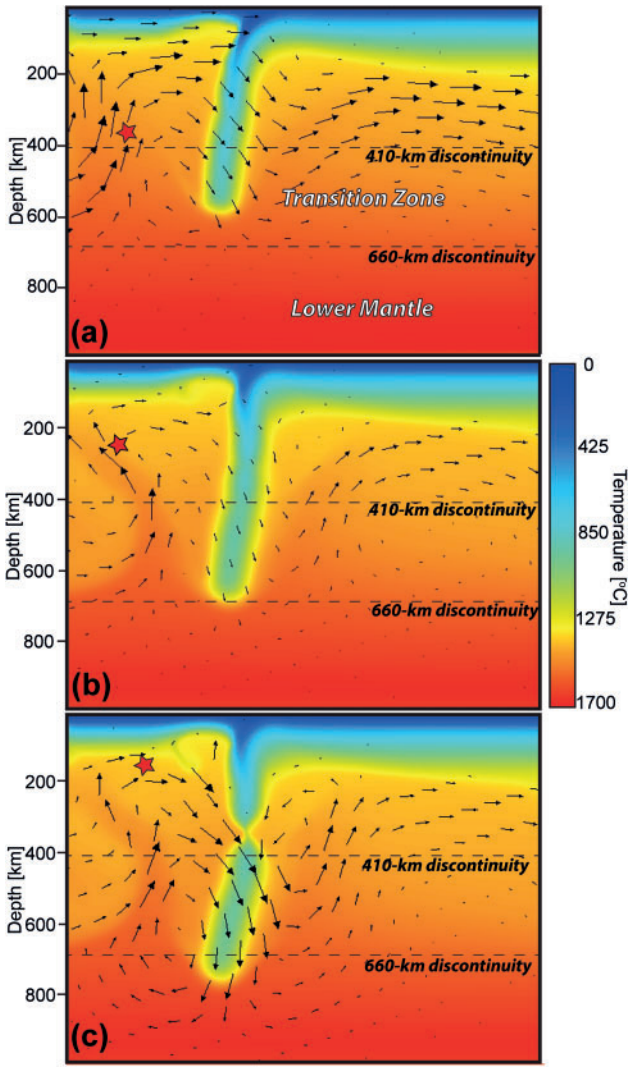

Fig. 12. Ascent of TZ material to lithospheric depths in a thermomechanical simulation of continental collision involving slab roll-back and break-off [modified from McGowan *et al.* (2015)]. The simulation begins with a 400 km long slab subducting at an angle of 45°. The red star indicates the path of a low-density passive tracer, which was at 520 km depth at the beginning of the simulation. No velocity boundary conditions are imposed; velocities are controlled entirely by the balance between internal forces (e.g. buoyancy, shear resistance). More details of the method have been given by Afonso & Zlotnik (2011); a video of the whole process is provided in Supplementary Data Fig. A1. (a) The concomitant subduction and steepening of the slab generates a large-scale passive upwelling down to the TZ. (b) This broad upwelling evolves into a narrower 'channel' (favored by a non-linear rheology) with velocities of the order of 3–8 cm a^{-1}. (c) Once the continental plate arrives at the trench, subduction slows down and slab break-off occurs. At this point, material initially at TZ depths has been brought up to lithospheric depths in <10 Myr, where it can become part of smaller-scale lithospheric tectonic processes.

Dobrzhinetskaya *et al.* (2009) clearly represent a disequilibrium microstructure, suggesting rapid reaction, inversion of stishovite to coesite, and quenching. Similarly, many of the spherules of metallic alloys separated from the chromitites display disequilibrium microstructures (Fig. 2), suggestive of unmixing and quenching, and some contain blades of graphite (Robinson *et al.*, 2004). Majoritic garnet, stable in the Transition Zone, could break down progressively during ascent of the harzburgites, hindering microstructural equilibration; rapid ascent and cooling in the final stages of uplift may explain the preservation of pseudomorphs (Fig. 7) in some rocks.

The answer to the question of how parts of the SSZ mantle could have reached TZ depths is more difficult, with ambiguous support from thermomechanical simulations. Geochemical and petrological evidence suggests that the chromitite-bearing harzburgites were formed in SSZ-type mantle, although the temperature and pressure conditions of formation are poorly constrained. We therefore suggest two (speculative) processes that potentially can result in the subduction of SSZ rocks into the Transition Zone.

In one scenario, the chromitite-bearing harzburgites are formed at relatively high temperatures within the mantle wedge, depleted by melting induced by fluids from the slab. This scenario resembles a widely accepted model for the formation of SSZ ophiolites (González-Jiménez *et al.*, 2014a). However, thermomechanical simulations suggest that this hot, buoyant mantle wedge is difficult to subduct. Wedge mantle would be forced to move towards the top of the slab, cool down, and be dragged down by the large-scale downward flow produced by the subducting slab (Fig. 13a). Although numerical simulations demonstrate that a significant volume of the mantle wedge can be carried down with the slab in this way, the chemical buoyancy of harzburgites compared with normal mantle wedge rocks would tend to resist the passive drag towards the TZ. However, it is plausible that the large-scale circulation produced by the subducting slab would overcome this positive buoyancy.

This scenario, however, poses another question: how do these harzburgitic bodies stay in the TZ for extended periods of time? There is no obvious reason why they should stay significantly cooler than the surrounding mantle while at TZ depths for hundreds of million years. Once they were thermally equilibrated, their chemical buoyancy would render them unstable and force them to return to shallower levels on relatively short time scales.

An alternative scenario that overcomes some of the above difficulties involves the erosion of old lithospheric mantle by direct or indirect action of the subducting slab. In this model (Fig. 13b) the oceanic plate is subducting below continental, rather than oceanic mantle; this is consistent with the Os-isotope evidence that the harzburgitic mantle represents ancient subcontinental lithospheric mantle (SCLM) (Table 4). Mechanical erosion of the lower parts of the lithospheric mantle of the overriding plate has been proposed to explain a variety of processes in subduction environments (e.g. Malavieille *et al.*, 2002; Humphreys *et al.*, 2003; Scholl & von Huene, 2007; Bao *et al.*, 2014; Froitzheim *et al.*,

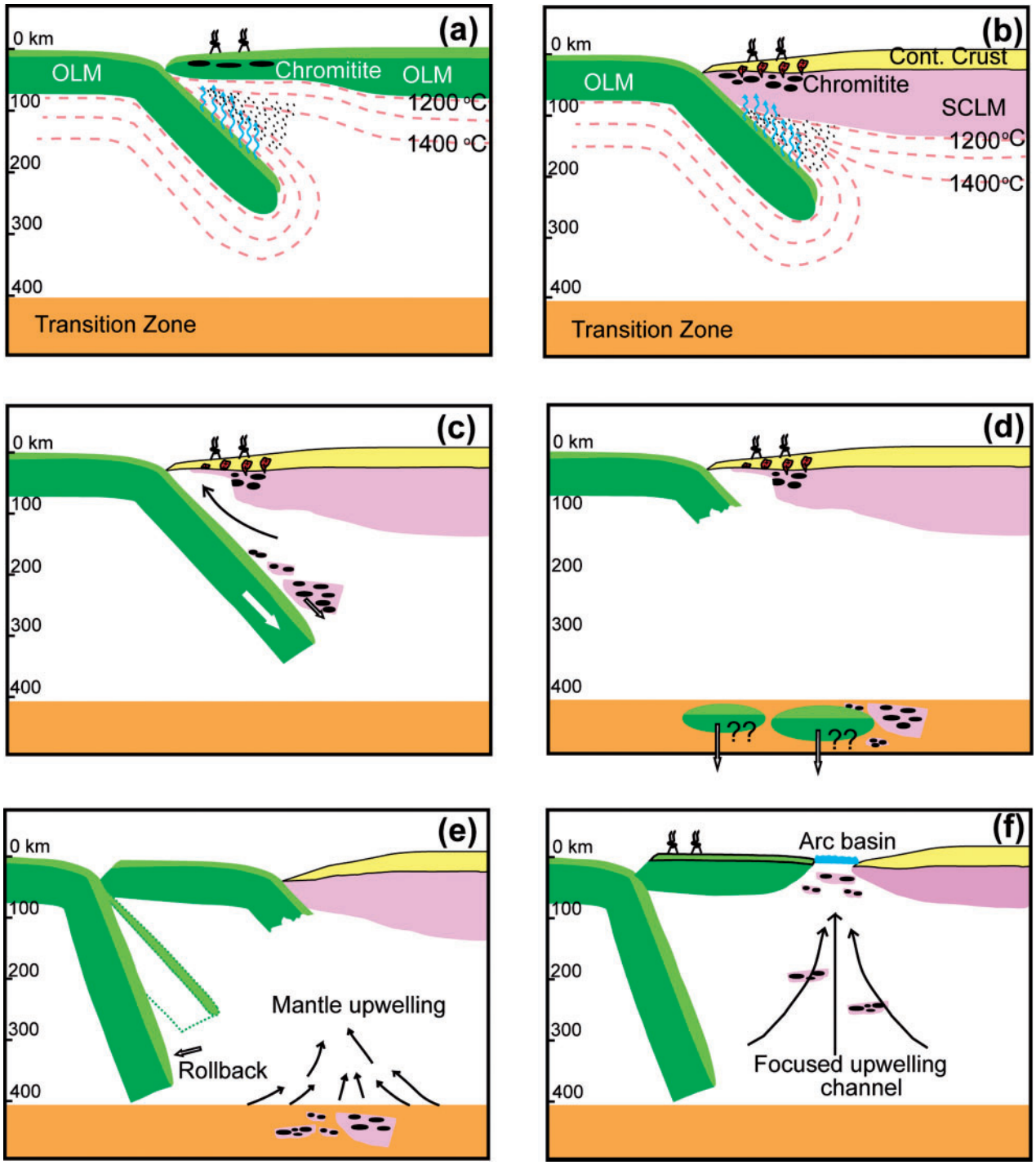

Fig. 13. Schematic illustration of the proposed evolution of the YZSZ peridotites. (a) Standard model for depletion of SSZ peridotites, and local formation of chromitites, by the infiltration of slab-derived fluids into the oceanic mantle wedge, inducing melting. Temperature field and flow lines are estimated from thermomechanical studies (see Fig. 12). As discussed in the text, this model produces hot, depleted (highly buoyant) volumes in the shallow part of the wedge, and a 'slip zone' along the top of the slab, both of which impede subduction of the peridotites and chromitites. (b) An alternative model, in which the subducting slab is in contact with a block of ancient SCLM, which is relatively cold and already depleted; chromitites and associated dunite channels are formed as in (a), by reaction of slab-derived fluids and melts, but in an overall cooler environment. (c) Subduction (*c.* 375 Ma) of both slab and detached SCLM mantle wedge into the Transition Zone. (d) Subducted SCLM resides in the Transition Zone for 100–200 Myr, heating to temperatures >1300 °C; the denser, less depleted slab may descend into the Lower Mantle. (e) Arrival and roll-back of a new slab promotes broad mantle upwelling (Moresi *et al.*, 2014), which rapidly develops into dynamic channelized upwelling that carries buoyant material up from the Transition Zone to shallow depths on short timescales (7–10 Myr; Afonso & Zlotnik, 2011; McGowan *et al.*, 2015). (f) Emplacement of rising harzburgitic mantle into a back-arc or forearc basin along the YZSZ during Jurassic or Cretaceous SSZ processes, forming new sea floor in some areas. Once in this position, the peridotites were subjected to repeated thrusting during the final closure of Neo-Tethys. OLM, oceanic lithospheric mantle; Cont., continental; SCLM, subcontinental lithospheric mantle.

2014) and it has been observed in numerical simulations (e.g. Arcay *et al.*, 2005; Sobolev & Babeyko, 2005).

Levander *et al.* (2014) have proposed the convective removal of continental margin SCLM by a subducting oceanic slab to explain geophysical data from NE South America and the Gibraltar arc; in these situations, as in our model, detached SCLM apparently is being subducted to depths of 250 km to > 500 km. Chemical modification by slab-released fluids may also assist in the destabilization of parts of the overriding lithospheric mantle (Humphreys *et al.*, 2003); this would be consistent with the formation of chromitites and their dunite envelopes within old, previously depleted and relatively cool SCLM (Shi *et al.*, 2012b). On average, these lower parts of the subcontinental lithosphere can be up to 250°C colder than a typical oceanic mantle wedge. Such thermal negative buoyancy readily counteracts the intrinsic chemical buoyancy of the SCLM, favouring its subduction into the TZ (Fig. 13c). Once at TZ depths, it would also take longer for these fragments of SCLM to become heated to the point of positive buoyancy, depending on the original size of the bodies (Fig. 13d). It should be noted that this process is not limited to collisional environments and, in principle, provides a general mechanism for carrying SSZ lithospheric material into the deep mantle.

Geological implications

Early ideas about the setting of the YZSZ ophiolites (Nicolas *et al.*, 1981; Pearce & Deng, 1988) were influenced by assumptions about the stratigraphic relationships between sedimentary and igneous units in the central and eastern parts of the suture zone. The overall paucity of mafic igneous rocks led to suggestions that the peridotite massifs represented oceanic lithosphere beneath slow-spreading ridges with low heat flow (Nicolas *et al.*, 1981). Girardeau *et al.* (1985*a*, 1985*b*) recognized that the Xigaze ophiolite, commonly cited as the most complete example of an 'ophiolite section' in the YZSZ, is not typical of mid-ocean spreading ridges, and suggested that it formed in a small intra-oceanic extensional basin. Later investigations stressed the tectonic contacts between most lithological units, and favored a complex arc–backarc (SSZ) setting, as in the case of most chromitite-bearing ophiolites (Aitchison *et al.*, 2003; Hebert *et al.*, 2003; Bedard *et al.*, 2009; Bezard *et al.*, 2011).

As more geochronological and geochemical data have accumulated, it has become apparent that along much of the YZSZ, mafic magmatism was confined to a short interval from about 130 to 120 Ma, and that the ultramafic rocks and the mafic rocks are isotopically distinct and probably unrelated (Gøpel *et al.*, 1984; Dai *et al.*, 2013). The ages of radiolarian cherts interbedded with and overlying the volcanic rocks in the Xigaze area suggest that this entire magmatic episode lasted only about 6 Myr (123–117 Ma; Ziabrev *et al.*, 1999, 2003). The generation of a spectrum of mafic rocks ranging from mid-ocean ridge basalt (MORB)-like to arc-like, all in one area and on such a short time scale, suggests a forearc setting, with rapid extension related to subduction initiation and rapid slab roll-back (Dai *et al.*, 2013; Moresi *et al.*, 2014). This is consistent with the model presented here, except that two similar episodes (*c.* 170–150 Ma and 130–120 Ma) may be required to produce the two age populations of ophiolites currently recognized.

This model also resolves some apparent conflicts in the geology and petrology of the YZSZ ophiolites. For example, the mafic rocks 'associated' (tectonically juxtaposed) with the YZSZ peridotites are Jurassic–Cretaceous in age and mainly have MORB affinities (Zhou *et al.*, 2002; Zhong *et al.*, 2006; Zhang *et al.*, 2005; other references have been given by Dai *et al.*, 2012, 2013). This is not easily reconciled with the petrology of the ultramafic rocks, which show a two-stage evolution with extreme depletion overprinted by an SSZ trace element signature (including the chromitites; Zhou et al., 1996, 2005, 2014). A similar situation is found in the Zedang area to the west, where MORB-like basalts (Zhang *et al.*, 2005) give Jurassic Sm–Nd ages (175 ± 20 Ma; Wei *et al.*, 2006) and radiolarian ages are Bathonian to late Callovian (161-168Ma ± 11 Ma; Aitchison *et al.*, 2007*b*) yet the peridotites display SSZ-type trace element signatures (Xia *et al.*, 2003; Hebert *et al.*, 2012). However, if the signatures of depletion and SSZ trace element enrichment in the harzburgites were inherited from ancient delaminated SCLM and a Devonian SSZ environment, as proposed here, there is no dilemma.

Aitchison *et al.* (2003; see also Bedard *et al.*, 2009) recognized that each of the peridotite massifs along the YZSZ appears to have originated in a range of (mainly SSZ) environments and at different locations; this is supported by paleomagnetic data (Abrajevitch *et al.*, 2005) and petrological studies (Hebert *et al.*, 2003, 2012; Liu *et al.*, 2012). This diversity is expected if the peridotite massifs represent 'random samples' of material emplaced into the Transition Zone at various times and places in the past, and excavated by one or more subduction systems during closure of the Neo-Tethys ocean.

Other models—questions and answers

The SuR-UHP mineral assemblage (Griffin *et al.*, 2013; Supplementary Data Table A1) was first ascribed to deep subduction (Bai *et al.*, 2001), but several later models do not recognize the constraints imposed by this mineralogy, focusing instead on the possibility of diamonds, in particular, being widespread in the asthenospheric mantle, or forming in subducted slabs (e.g. Yang *et al.*, 2007; Zhou *et al.*, 2014; Robinson *et al.*, 2015). However, this category of models is not consistent with evidence derived from the latest studies on these diamonds (Howell *et al.*, 2015). Their striking differences from kimberlitic diamonds make it unlikely that they are simply widespread components of the

mantle. Their high-*T* metallic inclusions are inconsistent with formation in a low-*T* slab environment; their N-aggregation characteristics argue against a long mantle residence; and their N-isotope characteristics suggest disequilibrium crystallization.

Another suite of models accepts the possibly Transition Zone nature of the mineralogy, but fails to supply a realistic explanation for the occurrence of SuR-UHP assemblages in both chromitites and peridotites. A common thread in such models (e.g. Yang *et al.*, 2014, 2015; Xiong *et al.*, 2015; Xu *et al.*, 2015) is that single chromite grains have crystallized from melts (and trapped their inclusions) in the Transition Zone, then have been carried up by fluids or 'plumes', and deposited as massive chromitites in the upper mantle. These models also face several problems.

(1) The crystallization of chromite from mafic or ultramafic melts in the Transition Zone is not consistent with available experimental evidence. Such melts are unlikely to be generated in the Transition Zone; the deepest komatiite-like melts are considered to come from depths of *c.* 330 km (Herzberg, 1992). Even if such melts did exist in the Transition Zone, they would not crystallize chromite; their liquidus phases would be majoritic garnet and pyroxene (Irifune, 1985; O'Neill *et al.*, 1993; Robin-Popieul *et al.*, 2012).

(2) Chromite, a very dense phase, is unlikely to be carried >400 km up through the mantle in melts or fluids. Komatiitic melts would be denser than the surrounding peridotite at $P > 13$ GPa, preventing their rise (Robin-Popieul *et al.*, 2012).

(3) The microstructures of the chromitites (Fig. 4; Satsukawa *et al.*, 2015) are consistent with metamorphism of the chromitites in the Transition Zone, and grain growth during ascent, but not with the rise of single chromite grains, or even small volumes of chromitite. All evidence indicates that the massive chromitites, some of which form very large ore bodies, were exhumed as coherent volumes of rock, protected by their envelopes of dunite and harzburgite. The exsolution structures consistent with Transition Zone metamorphism have now been found in massive, nodular and disseminated chromites (Fig. 3), confirming a similar history for all types of chromite.

(4) The most probable models for chromitite formation involve shallow processes, with mixing or mingling of magmas, and sedimentation and transport of chromite–olivine aggregates (see review by González-Jiménez *et al.*, 2014*a*, 2014*b*); this is consistent with the O- and Hf-isotope signatures of the magmatic zircons described by McGowan *et al.* (2015).

(5) The major and minor element compositions of the chromitites with the SuR-UHP mineral inclusions are indistinguishable from those of chromitites formed in shallow ophiolitic environments.

(6) The same SuR-UHP phases are found in the chromitites, in their host peridotites, in peridotites in which chromitites have not been reported (Yang *et al.*, 2014) and in pyroxenites within these peridotites (Xiong, 2015). This observation is not accounted for by models that depend on the igneous crystallization of chromite in the Transition Zone.

'Crustal' minerals in peridotites and chromitites

The mineral separates from the chromitites (and peridotites) contain many 'crustal' minerals (zircon, quartz, corundum, K-feldspar, plagioclase, apatite, amphibole, rutile, titanite, kyanite, andalusite, almandine garnet; Robinson *et al.*, 2015). Corundum contains inclusions of the SuR-UHP assemblages (Xu *et al.*, 2015), but the other phases are clearly not of high-*P* origin. The ages of the separated zircons span a very wide range (Fig. 8c). Various explanations have been proposed, including the ubiquitous presence of recycled crustal material in the upper mantle (Yamamoto *et al.*, 2013); this would not seem to explain the presence of low-*P* phases in samples with evidence of a possible Transition Zone history. Robinson *et al.* (2015) proposed that the chromitites and peridotites were contaminated by slab-derived fluids, which is difficult to reconcile with the preservation of the Transition Zone microstructures described above.

However, the presence of these crustal minerals poses a problem for the proposed model only if it is assumed that they were present in the peridotites before their deep subduction. Although there is little or no information on the petrographic context of most of these minerals, age data from zircons can provide some insights. Belousova *et al.* (2014) have demonstrated that zircon populations in the ophiolitic rocks of the Coolac Belt in SE Australia match those in the surrounding S-type granites, including both the magmatic population and the inherited ones. They concluded that all of the zircons were physically introduced into the ophiolitic rocks by melts or fluids derived from the granites, during and after emplacement. A similar situation is suggested by the presence, in the Luobusa chromitite and other bodies, of zircons with concordant ages that are 10–30 Myr younger than the accepted ages of the emplacement of the 'ophiolites' (Yamamoto *et al.*, 2013; Fig. 8c). This suggestion is supported by the similarities between the zircon age spectra shown by Yamamoto *et al.* (2013) and Robinson *et al.* (2015) and those from Jurassic–Cretaceous sediments (zircons recycled from still older sediments) and igneous rocks of the Lhasa area (Leier *et al.*, 2007; Wu *et al.*, 2010; Aitcheson *et al.*, 2011; Fig. 8d and e). This could be further tested by integrating zircon Hf-isotope data with the U–Pb ages.

The YZSZ ophiolites are intruded by dikes (some felsic; plagiogranites, adakites, quartz diorites) that cut both the mantle rocks and the mafic parts of the sections. Additionally, some of the ophiolites have been thrust over, and interleaved with, felsic rocks of the Gangdese batholith and Triassic to Cretaceous sediments at various stages in their complex emplacement history (Aitchison *et al.*, 2003). This tectonic activity could have provided opportunities for the ultramafic

rocks and chromitites to be contaminated with crustal material during and after their emplacement in the crust. Some of our samples have yielded calcic plagioclase and rare grains of amphibole. Liu *et al.* (2010) argued that these phases represent relatively shallow (i.e. late-stage) infiltration of the peridotites by subduction-related melts of the types described by Bezard *et al.* (2011), whereas Borisova *et al.* (2012) have described veins of diopside + anorthite in the Oman ophiolite, related to high-T ($\geq$900°C) hydrothermal activity. It therefore appears probable that the 'crustal' minerals in the chromitites and peridotites represent syn- to post-emplacement natural contamination.

However, there are still unresolved problems with regard to some 'crustal' phases that we interpret as pre-subduction.

(1) Synthetic $ZrSiO_4$ inverts to a scheelite-structured polymorph (reidite) at high P and T [variously estimated at 12–15 GPa at 900°C (Reid & Ringwood, 1969; Liu, 1979) or at 8–10 GPa at 900–1400 °C (Ono *et al.*, 2003)]. The euhedral zircons (Fig. 8) with 375 Ma ages, separated from a massive chromitite, should have gone through this transition. However, it is not clear that these experimental results on pure $ZrSiO_4$ are applicable to natural zircons with high contents of Hf (1 wt %) and REE. It also is not clear how this transformation could happen without obliterating the magmatic zoning in the zircons (Fig. 8), although it does not involve any change in the coordination of Si and Zr, and might be easily reversed.

(2) These zircons also might be expected to show disturbed U–Pb systems owing to the high T predicted from the model, but most define a single concordant age (McGowan *et al.*, 2015). However, magmatic zircons commonly retain ages to very high T; high P might also tend to inhibit the loss of Pb, although this has not been tested experimentally.

(3) The same zircons have euhedral prisms of fluorapatite (3–4% F) on their crystal faces, and as inclusions (Fig. 8a); these should have broken down to $Ca_3(PO_4)_2$ at $>$13 GPa at *c.* 1300°C (Murayama *et al.*, 1986). We could suggest that the apatite may be stabilized to higher P by high contents of REE and Sr, but note that the reaction is also easily reversible. The apatite crystals have not yet been examined by TEM to see if they show any indication of recrystallization.

Corundum, SiC and super-reducing conditions

Assemblages such as SiC + Si imply 'super-reducing' conditions with fO_2 well below the iron–wüstite (IW) buffer, which is commonly considered as a limiting value for the deep mantle (Frost & McCammon, 2008). This raises the question of how to generate such low fO_2, and where on the P–T path these conditions might have been relevant. Low fO_2 in the Transition Zone is suggested by the presence of native Fe coupled with the high levels of Fe^{3+} (micro-Møssbauer spectroscopy) in the massive chromitites that show diopside/coesite exsolution (Ruskov *et al.*, 2010; McGowan *et al.*, 2015); this is consistent with the dissociation reaction $Fe^{2+} \rightarrow Fe^{3+} + Fe^0$. Ruskov *et al.* (2010) regarded the high levels of Fe^{3+} in the massive chromites as evidence that the chromites were in the CF structure at the time, as this structure can accommodate more Fe^{3+} than the cubic structure. O'Neill *et al.* (1993) suggested that the Transition Zone may represent a shell with low fO_2 between the more oxidized upper and lower mantle, but envisioned fO_2 near the IW buffer ('metal saturation').

Some of the native elements in the SuR-UHP assemblage (Ni, Co, Fe) do not require fO_2 below the IW buffer, but others such as Ti and Cr (Supplementary Data Table A1; Yang *et al.*, 2015) imply fO_2 even lower than Si–SiC at low T. However, at higher temperatures these native elements can exist under relatively less reducing conditions; for the Transition Zone temperatures estimated above (1300 to $>$1500°C), the required fO_2 is in the same range as Si–SiC (IW –4 to –6). Understanding the processes that generate these conditions is still a challenge; we suggest that they may reflect the introduction (and disassociation) of CH_4 from the deeper Earth, and that this influx may have been limited to discrete channels or other structures, producing a patchwork of variable P–T–fO_2 conditions. This aspect of the problem cannot be rigorously addressed until more detailed constraints from coexisting phases are available.

Corundum is relatively common in mineral separates from some YZSZ localities, occurring as crystal fragments up to several millimeters long; some of the more unusual phases reported from the chromitites (e.g. silicides, carbides, nitrides) occur as inclusions in corundum (Xu *et al.*, 2015). This raises the question of where, and when in the history of the peridotites, these SuR conditions have occurred. In a remarkable parallel, corundum (sapphire, ruby and non-gem corundum) is associated with coarse-grained moissanite (SiC) in the Rakefet mafic igneous complex at Mt Carmel (Israel) and associated alluvial deposits (Roup *et al.*, 2009). Crystals of SiC range up to 4·1 mm in size; we have documented both 4H and 6H polytypes using Raman spectroscopy (Huang *et al.*, in preparation). The non-gem corundum contains abundant inclusions of phases requiring very low fO_2, including native V, TiC and TiN. The geological situation suggests a shallow ($<$150 km) origin (Apter, 2014; Toledo *et al.*, 2015). The similarities in mineral assemblage allow us to speculate that the corundum, and potentially much of the SuR assemblage, may represent conditions reached within the peridotite or chromitite rocks of the Luobusa massif at relatively shallow depths during their ascent.

Preservation of macroscopic structures

Macroscopic structures typical of ophiolitic chromitites (modal banding, transitions from massive to nodular to disseminated chromitite, chromite pods with dunite selvedges) are preserved in many parts of the Luobusa chromitites (see Xu *et al.*, 2011; Xiong *et al.*, 2015).

Preservation of these structures during the subduction–exhumation history proposed here may seem improbable to structural geologists. However, several points are worth making in this context.

(1) Some massive chromitites show clear evidence of internal high-*P* deformation and grain growth (Fig. 4) although the macroscopic structures remain apparently undisturbed. Similarly, single nodules in the nodular chromites typically consist of a few large crystals, suggesting metamorphic recrystallization.

(2) Many of the chromitites, and especially the peridotites, have been strongly deformed and recrystallized at low pressures (A-type lattice-preferred orientation; dominant (010)[100] slip system), producing coarse-grained, coarsely foliated or lineated rocks (Girardeau *et al.*, 1984; Xu & Jin, 2010).

(3) In the model proposed here, the peridotite bodies would be carried up within rapidly upwelling mantle, aided by their own buoyancy. In this situation, as noted above, strain will be concentrated at the interface between the harzburgite massif and the surrounding more ductile asthenosphere. This can protect the interior of the body from major deformation and fluid access during the mantle portion of its journey. It may be significant that the largest massifs, such as Purang, are generally very fresh.

(4) It important to recognize that the less deformed domains (those commonly illustrated) represent strain shadows in mantle-derived tectonites, and, as such, provide valuable insights into the history of these ultramafic bodies; we can regard them as windows into the past.

Ophiolitic crust–mantle sections

There are no known exposures of traditional UHP rocks, such as eclogites, among the ophiolites of the YZSZ, despite the evidence that some peridotites and chromitites have a (very) UHP history. In our model, this is explained by the subduction of ancient SCLM, which would not carry oceanic crust, and by the probability that any associated mafic material, once converted to eclogite during subduction, would be more likely to sink into the lower mantle, rather than rise to the surface (Afonso & Zlotnik, 2011). It has been suggested that arguments for a high-pressure history for the ultramafic rocks are inconsistent with the preservation of complete ophiolite sections in these ultramafic rocks (see Yang *et al.*, 2007, and references therein). There are two aspects to this question. One relates to the existence of such sections; the other is the relevance of such sections, if they do exist.

The classical definition of an ophiolite section (the 'Penrose model'; Anonymous, 1972) includes a basal section of mantle peridotite, overlain successively by ultramafic to mafic cumulates, a sheeted dike complex, pillow lavas and a sedimentary section, usually containing deep-water rocks including radiolarian cherts. The 'type examples' are the Troodos and Semail ophiolites. The ophiolites of the Xigaze area in the central YZSZ are commonly cited (Girardeau *et al.*, 2004; Bao *et al.*, 2013) as examples of a 'complete section'. However, the earliest descriptions in western literature (Nicolas *et al.*, 1981) recognized that the Xigaze rocks represent 'a peculiar oceanic lithosphere', noting the scarcity of mafic volcanic rocks and the lack of a sheeted dike complex (but the presence of 'sheeted sills'). Our observations of the 'sheeted sills' in the Dazhuka section SE of Xigaze indicate that these consist of thinly layered gabbros cut by dolerite dikes, but with no clear evidence of the chilled margins implied by the term 'sheeted'. Pillow lavas also have been mapped locally, but may be in tectonic, rather than stratigraphic, contact with the mantle rocks (Aitchison *et al.*, 2003). The description of this area as containing a 'complete ophiolite section' floored by ultramafic rocks also rests partly on the earlier identification of the Cretaceous sediments of the Xigaze group as part of such a section. Although the Xigaze sediments may be in depositional contact with some mafic rocks (including pillow lavas) of the area (Hu *et al.*, 2008; Wang *et al.*, 2010, 2012; An *et al.*, 2014), these contacts also have been described as tectonic (Aitchison *et al.*, 2003). Furthermore, there are apparently no clear depositional contacts between the mafic volcanic rocks and the peridotite massifs or the gabbro sections. Wu *et al.* (2014) have presented an extensive summary, concluding that there are no genetic relationships between the peridotite massifs and the associated mafic igneous rocks of the YZSZ.

The Luobusa massif has also been described (Zhou *et al.*, 1996) as having a 'complete section'. However, this appears to be based mainly on an extensive unit, labeled as 'cumulate rocks', that features on many published maps (Xu *et al.*, 2011, 2015; Xiong *et al.*, 2015). Yamamoto *et al.* (2007) showed that this unit is a serpentinite mélange with scattered blocks of gabbro and basalt. A small area of layered gabbros is in fault contact with peridotite at the western end of the massif. Other evidence cited is an inferred stratigraphic relationship (Malpas *et al.*, 2003) with Middle Jurassic mafic rocks (155 to >160 Ma; McDermid *et al.*, 2002) of the Zedang Terrane; this is now recognized as a distinct tectonic block separated from the ultramafic rocks by Miocene thrust faults (Aitchison *et al.*, 2003). Hebert *et al.* (2012) have stressed the distinction between 'dismembered' (mainly Jurassic) and 'non-dismembered' (largely Cretaceous) ophiolites in the YZSZ. However, even in 'non-dismembered' examples all the described contacts appear to be tectonic (Aitchison *et al.*, 2003), and 'overlying units' commonly are separated by many kilometers along the strike of major faults; there is a danger that sections inferred from this type of data may be constructs, rather than reflecting genetic relationships.

However, even if mafic rocks and sedimentary successions did overlie some of the peridotite bodies prior to thrusting and transcurrent faulting, this would not be inconsistent with the proposed model, in which the

peridotite massifs were exhumed from the Transition Zone into a zone of extension, which developed into small ocean basins. We suggest that this buoyancy-driven emplacement could finally bring the massifs to the surface, leaving them exposed at the paleo sea floor. Liu *et al.* (2014) have invoked the concept of 'oceanic core complexes' forming seamounts, to explain the high paleo-elevation suggested by the lack of mafic rocks or sedimentary cover on the Purang massif (western YZSZ; Niu *et al.*, 2015; see also Liu *et al.*, 2015). Our model also invokes buoyancy-driven tectonics, but involving much deeper mantle levels. These exhumed massifs would then serve as the 'basement' to any mafic volcanism, or oceanic sedimentation, that followed their emplacement. The heat delivered by the upwelling mantle may be closely linked to the (relatively sparse) mafic magmatism that accompanied and followed their emplacement.

There are strong similarities between the collision–extension history that has defined the setting of the YZSZ peridotites and the tectonic development of the Betic Cordillera of southern Spain–northern Africa. Vissers *et al.* (1995) described the Cordillera as 'a clear example of a collisional orogen that has undergone large-scale extensional collapse while convergent motion of the bounding plates continued'. They showed that the peridotitic massifs of the region reflect multistage upwelling of upper mantle from asthenospheric depths to the surface; these bodies include the formerly diamondiferous rocks of the Beni Boussera massif (Pearson *et al.*, 1993) and the Ronda massif, in which pyroxene–spinel symplectites after majoritic garnet have been described (Tubía *et al.*, 2004).

Origins of the peridotites

Whole-rock Re–Os model ages (T_{DM}) of peridotites from the YZSZ range from Archean (3·4 Ga) to values expected for the convective mantle near the time of emplacement (Supplementary Data Table A4; Fig. 10c). In general, the older ages are found in the more depleted harzburgites and the younger, depleted-mantle ages in the lherzolites (Shi *et al.*, 2012a; Xiong, 2015); however, young ages are also found in some harzburgites. Many of these younger model ages may represent mixtures of several generations of sulfides and/or PGM [see review by González-Jiménez *et al.* (2014a)] and thus will represent minimum ages for the depletion of the peridotites. *In situ* analyses of PGM can be more useful than whole-rock analyses in identifying possible episodes of melting and metasomatism (Griffin *et al.*, 2004), and some samples have yielded well-defined age populations that may represent specific events or processes. Shi *et al.* (2007) identified a population of large (200 μm) Os–Ir nuggets in the Luobusa chromitites with $T_{RD} = 230 \pm 30$ Ma, and another at $T_{RD} = 240 \pm 30$ Ma in the chromitites of the Dongqiao massif within the older Bangong–Nujiang suture zone to the north. However, the Dongqiao samples also contain another population of more complex PGM with T_{RD} ages clustered around 0·9 and 1·1 Ga (Supplementary Data Table A4), suggesting that the protoliths were lithospheric mantle that was at least Neoproterozoic in age.

These model ages suggest that at least some of the harzburgites may represent pieces of ancient SCLM, either eroded from a colliding continent (Fig. 13b) or stranded in the ocean basins during rifting episodes. An analogy would be the unroofing of continental lithosphere to produce the ultramafic basement of the Ligurian ophiolites of northern Italy (Rampone *et al.*, 2005). The 325–375 Ma U–Pb zircon ages and Os-isotope model ages of laurites (McGowan *et al.*, 2015; Table 4) are similar to the ages of some ocean island basalt (OIB)-type gabbros in the YZSZ (364 ± 2 Ma; Dai *et al.*, 2011); this may suggest that some of this rifting and subsequent subduction (Fig. 13b) took place in the Paleo-Tethys ocean, before transport of the subducted SCLM wedge materials into the Transition Zone (Fig. 13b) and their metamorphism within the Transition Zone at ~240–230 Ma (Fig. 13c).

The Tethyan subduction in the Jurassic (~170–150 Ma) may have disturbed previously subducted lithospheric materials in the Transition Zone, and excavated them to shallow levels to form the harzburgitic lithosphere (Fig. 13e and f) that is now preserved in the Luobusa–Kangjinla massif. This excavation process may also have occurred during the early Cretaceous (~130–120 Ma). Garnet amphibolites within the ophiolite mélanges have Ar–Ar cooling ages of *c.* 125 Ma; estimated protolith ages are *c.* 135 Ma. These amphibolites have been interpreted either as the soles on which the peridotites were thrust onto the crust (Guilmette, 2005; Guilmette *et al.*, 2008, 2009) or as another late thermal event in the history of the peridotites (e.g. Wakabashi & Dilek, 2000). In either case, after emplacement and accompanying serpentinization, the peridotites were extensively intruded by dolerites, part of the widespread 130–120 Ma magmatic event mentioned above. This scenario is consistent with the short 'rise time' (7–10 Myr) modeled for the ascent of the peridotites from the TZ to the surface. The mafic magmatism in the area would thus have begun in the late stages of exhumation, consistent with the heat input expected from rapid, channelized upwelling of the mantle. During the later dismemberment of the ophiolite complexes by strike-slip faulting and compression (Dubois-Cote *et al.*, 2005; Hebert *et al.*, 2012), the dry, rigid and buoyant harzburgite massifs might have survived more easily than the lherzolitic oceanic mantle, and thus would now be 'over-represented' in the YZSZ.

In the model presented here, there is no specific relationship between the timing of the original extension–subduction process that emplaced shallow mantle material in the TZ and its later excavation by slab roll-back. The model permits single or multiple events with variable residence times in the lower upper mantle or Transition Zone. The Transition Zone may indeed be a

'slab graveyard', full of ancient subducted material awaiting resurrection by slab roll-back.

CONCLUSIONS

Agee (1999) noted that 'geologists have never held a proven, unadulterated piece of the Transition Zone in their hands'; we think this may finally be possible.

The mineralogical and microstructural data summarized here suggest that the Luobusa–Kanjingla–Zedang peridotite massif ('ophiolite') represents a fragment of ancient SCLM that was modified in an SSZ environment. This modification included both extreme depletion and the formation of podiform chromitites similar to those observed in many ophiolite complexes. This mantle fragment apparently was subducted into the lower upper mantle or Transition Zone (~410–660 km depth), heated to temperatures >1300°C and perhaps >1500°C, and recrystallized to UHP phases including wadsleyite, a new cubic Mg-silicate, majoritic garnet and CF-structured chromite. It was then rapidly exhumed by dynamic, focused mantle upwelling produced by roll-back of a later subducting slab, stalled in the Transition Zone. During this process (majoritic) garnet peridotites were converted to spinel peridotites, leaving only symplectitic intergrowths of opx + spinel ± cpx as reminders of their deeper history. The currently known distribution of the majoritic garnet symplectites suggests that other peridotite massifs in the YZSZ may have experienced a similar history. This scenario quantifies a previously undocumented large-scale tectonic process [similar to that envisaged by Arai (2010, 2013)], with major implications for mantle circulation and dynamics.

Many of the Tibetan peridotites, following their exhumation from the Transition Zone, may have acted as the 'basement' to younger igneous and sedimentary rocks, although not in the sense of the classic 'Penrose' ophiolite model. Our model can resolve many of the contradictions inherent in earlier ideas about the origin of the YZSZ 'ophiolites', and can help to integrate apparently disparate datasets.

The SuR-UHP mineral assemblage has been documented from six other peridotite massifs in the YZSZ, the Ray-Iz massif in the Polar Urals, and the Myitkina massif in Myanmar (Yang *et al.*, 2014). Except for the symplectites after majoritic garnet, the critical Transition Zone indicators identified here have not been reported from these other massifs, and more detailed studies are required to establish their presence or absence, especially in those from which diamond has been reported (Fig. 1). However, the processes identified here may be a relatively common feature of major continental collision zones.

There are still many questions to be answered. Re-evaluation of key field relationships, careful definition of trace-mineral equilibrium assemblages and their constraints on physical parameters, and precise *in situ* geochronology of key phases (zircon, PGM) are required to solve these. The nature, timing and *P–T* conditions of the low-fO_2 event(s) recorded by the SuR-UHP phases need to be established in detail to understand the role and nature of fluid phases at different levels of the mantle. There is considerable scope for experimental studies of the stability fields of key UHP phases and polymorphs, and the kinetics of N aggregation in diamond, to provide further tests of the model. These peridotite massifs appear to offer a new window into processes from the Transition Zone to the surface, and into a geodynamic process that may be a characteristic of major tectonic collision zones.

ACKNOWLEDGEMENTS

We thank Ba Dengzhu for sharing his experience and insights on Tibetan peridotites and chromitites (especially regarding the absence of ophiolitic crust–mantle sections). Howard Coopersmith, Dave Apter and Vered Toledo have given their enthusiastic collaboration on the Mt Carmel material referred to in this study. Jin Zhen-Min and Zhang Yanfei provided fruitful discussions on their experimental studies of chromite polymorphs and geochemistry. Steve Craven gave invaluable assistance with the selFrag work. Jonathon Aitchison and Paul Robinson are thanked for helpful discussions on Tibetan geology; Paul Robinson also provided Fig. 5a, from his long-term work on the Luobusa mineral separates. We are very grateful to Zheng Jianping for many discussions and our long-term collaboration, including his rigorous supervision of Xiong Qing's co-tutelle PhD thesis work. Hu Xiumian provided illuminating discussions of the relations between sedimentology and tectonics along the YZSZ.

FUNDING

This work was funded by a Foundation Grant from the ARC Centre of Excellence for Core to Crust Fluid Systems (CCFS), with additional support from the Institute of Tibetan Plateau Research, Chinese Academy of Sciences (Beijing). Analytical data were obtained using instrumentation funded by DEST Systemic Infrastructure Grants, ARC LIEF, NCRIS, industry partners and Macquarie University. This is publication 704 from the ARC Centre of Excellence for Core to Crust Fluid Systems (http://www.ccfs.mq.edu.au), and 1057 from the GEMOC Key Centre (http://www.gemoc.mq.edu.au).

SUPPLEMENTARY DATA

Supplementary data for this paper are available at *Journal of Petrology* online.

REFERENCES

Abrajevitch, A., Aitchison, J. C., Ali, J. R., Ba, D., Davis, A. M., Liu, J. B. & Ziabrev, S. V. (2005). Neotethys and the

India–Eurasia collision: insights from a palaeomagnetic study of the Dazhuqu ophiolite, southern Tibet. *Earth and Planetary Science Letters* **233**, 87–102.

Afonso, J. C. & Zlotnik, S. (2011). The subductibility of continental lithosphere. In: Brown, D. & Ryan, P. D. (eds) *Arc–Continent Collision. Frontiers in Earth Sciences*. Springer, pp. 53–86.

Afonso, J. C., Zlotnik, S. & Fernandez, M. (2008). The effects of compositional and rheological stratifications on small-scale convection under the oceans: implications for the thickness of oceanic lithosphere and seafloor flattening. *Geophysical Research Letters* **35**, L20308.

Agee, C. B. (1999). Phase transformations and seismic structure in the upper mantle and transition zone. In: Hemley, R. J. (ed.) *Ultrahigh-Pressure Mineralogy. Mineralogical Society of America and Geochemical Society, Reviews in Mineralogy and Geochemistry* **37**, 165–203.

Aitchison, J. C., Abrajevitch, A., Ali, J. R., Badengzhu, Davis, A. M., Luo, H., Liu, J. B., McDermid, I. R. C. & Ziabrev, S. (2002). New insights into the evolution of the Yarlung Tsangpo suture zone, Xizang (Tibet), China. *Episodes* **25**, 90–94.

Aitchison, J. C., Davis, A. M., Abrajevitch, A. V., Ali, J. R., Ba, D., Liu, J., Luo, H., McDermid, I. R. C. & Ziabrev, S. V. (2003). Stratigraphic and sedimentological constraints on the age and tectonic evolution of the Neotethyan ophiolites along the Yarlung Tsangpo suture zone, Tibet. In: Dilek, Y. & Robinson, P. (eds) *Ophiolites in Earth History. Geological Society, London, Special Publications* **218**, 147–164.

Aitchison, J. C., Ali, J. R. & Davis, A. M. (2007a). When and where did India and Asia collide? *Journal of Geophysical Research* **112**, B05423.

Aitchison, J. C., McDermid, I. R. C., Ali, J. R., Davis, A. M. & Zyabrev, S. V. (2007b). Shoshonites in southern Tibet record Late Jurassic rifting of a Tethyan intra-oceanic island arc. *Journal of Geology* **115**, 197–213.

Aitchison, J. C., Xia, X. P., Baxter, A. T. & Ali, J. R. (2011). Detrital zircon U–Pb ages along the Yarlung–Tsangpo suture zone, Tibet: Implications for oblique convergence and collision between India and Asia. *Gondwana Research* **20**, 691–709.

An, W., Hu, X., Garzanti, E., BouDagher-Fadel, M., Wang, J. & Sun, G. (2014). Xigaze forearc basin revisited (South Tibet): Provenance changes and origin of the Xigaze ophiolite. *Geological Society of America Bulletin* **126**, 1595–1613.

Anonymous (1972). Penrose field conference on ophiolites. *Geotimes* **17**, 22–24.

Apter, D. (2014). High pressure indicator minerals from the Rakefet Magmatic Complex (RMC), Mt. Carmel, Israel. Geological Society of South Africa, *Proceedings of the GSSA Kimberley Diamond Symposium* (Extended Abstract Poster No. 27)

Arai, S. (2010). Possible recycled origin for ultrahigh-pressure chromitites in ophiolites. *Journal of Mineralogical and Petrological Sciences* **105**, 280–285.

Arai, S. (2013). Conversion of low-pressure chromitites to ultrahigh-pressure chromitites by deep recycling: a good inference. *Earth and Planetary Science Letters* **379**, 81–87.

Arcay, D., Trice, E. & Doin, M. P. (2005). Numerical simulations of subduction zones: Effect of slab dehydration on *the mantle wedge dynamics. Physics of the Earth and Planetary Interiors* **149**, 133–153.

Bai, W., Zhou, M.-F. & Robinson, P. T. (1993). Possible diamond-bearing mantle peridotites and podiform chromitites in the Luobusa and Donqiao ophiolites, Tibet. *Canadian Journal of Earth Sciences* **30**, 1650–1659.

Bai, W., Yang, J., Robinson, P., Fang, Q., Zhang, Z., Yan, B. & Hu, X. (2001). Study of diamonds from chromitites in the Luobusa ophiolite, Tibet. *Acta Geologica Sinica* **75**, 404–409 (in Chinese with English abstract).

Bao, P., Su, L., Wang, J. & Zhai, Q. (2013). Study on the tectonic setting for the ophiolites in Xigaze, Tibet. *Acta Geologica Sinica* **87**, 395–425 (in Chinese with English abstract).

Bao, X., Eaton, D. W. & Guest, B. (2014). Plateau uplift in western Canada caused by lithospheric delamination along a craton edge. *Nature Geoscience* **7**, 830–833.

Bedard, E., Hebert, R., Guilmette, C., Lesage, G., Wang, C. S. & Dostal, J. (2009). Petrology and geochemistry of the Saga and Sangsang ophiolitic massifs, Yarlung Zangbo Suture Zone, southern Tibet: Evidence for arc–back-arc origin. *Lithos* **113**, 48–67.

Belousova, E. A., González Jiménez, J. M., Graham, I., Griffin, W. L., O'Reilly, S. Y., Pearson, N., Martin, L. & Craven, S. (2014). The enigma of crustal zircons in upper mantle rocks: clues from the Coolac ultramafic complex, SE Australia. *Geology* **43**, 123–126.

Bezard, R., Hebert, R., Wang, C., Dostal, J., Dai, J. & Zhong, H. (2011). Petrology and geochemistry of the Ziugugabu ophiolitic massif, western Yarlung Zangbo suture zone, Tibet. *Lithos* **125**, 347–367.

Bockrath, C., Ballhaus, C. & Holzheid, A. (2004). Stabilities of laurite RuS_2 and monosulphide liquid solution at magmatic temperature. *Chemical Geology* **208**, 265–271.

Borisova, A. Y., Ceuleneer, G., Kamenetsky, V. S., Arai, S., Bejina, F., Abily, B., Bindeman, I. N., Polve, M., De Parseval, P., Aigou, T. & Pokrovski, G. S. (2012). A new view on the petrogenesis of the Oman ophiolite chromitites from microanalyses of chromite-hosted inclusions. *Journal of Petrology* **53**, 2411–2440.

Brenan, J. M. & Andrews, D. (2001). High-temperature stability of laurite and Ru–Os–Ir alloy and their role in PGE fractionation in mafic magmas. *Canadian Mineralogist* **39**, 341–360.

Chan, G. H. N., Aitchison, J. C., Crowley, Q. G., Horstwood, M. S. A., Searle, M. P., Parrish, R. R. & Chan, J. S. L. (2015). U–Pb zircon ages for Yarlung Tsangpo suture zone ophiolites, southwestern Tibet and their tectonic implications. *Gondwana Research* **27**, 719–732.

Chen, M., Shu, J., Mao, H., Xie, X. & Hemley, R. J. (2003). Natural occurrence and synthesis of two new postspinel polymorphs of chromite. *Proceedings of the National Academy of Sciences of the USA* **25**, 14651–14654.

Corgne, A., Armstrong, L. S., Keshav, S., Fei, Y. W., McDonough, W. F., Minarik, W. G. & Moreno, K. (2012). Trace element partitioning between majoritic garnet and silicate melt at 10–17 GPa: Implications for deep mantle processes. *Lithos* **148**, 128–141.

Dai, J., Wang, C. & Li, Y. (2012). Relicts of the Early Cretaceous seamounts in the central–western Yarlung Zangbo Suture Zone, southern Tibet. *Journal of Asian Earth Sciences* **53**, 25–37.

Dai, J., Want, C., Polat, A., Santosh, M., Li, Y. & Ge, Y. (2013). Rapid forearc spreading between 130 and 120 Ma: Evidence from geochronology and geochemistry of the Xigaze ophiolite, southern Tibet. *Lithos* **172–173**, 1–16.

Dai, J.-G., Wang, C.-S., Hebert, R., Li, Y. L., Zhong, H. T., Guillaume, R., Bezard, R. & Wei, Y. S. (2011). Late Devonian OIB alkaline gabbro in the Yarlung Zangbo Suture Zone: Remnants of the Paleo-Tethys? *Gondwana Research* **19**, 232–243.

Dilek, Y. & Furnes, H. (2011). Ophiolite genesis and global tectonics: Geochemical and tectonic fingerprinting of ancient oceanic lithosphere. *Geological Society of America Bulletin* **123**, 387–411.

Dobrzhinetskaya, L. F., Wirth, R., Yang, J. S., Ian, D., Hutcheon, P. K. & Green, H. W. (2009). High-pressure highly reduced

nitrides and oxides from chromitite of a Tibetan ophiolite. *Proceedings of the National Academy of Sciences of the USA* **106**, 19233–19238.

Dubois-Cote, V., Hebert, R., Dupuis, C., Wang, C. S., Li, Y. L. & Dostal, J. (2005). Petrological and geochemical evidence for the origin of the Yarlung Zangbo ophiolites, southern Tibet. *Chemical Geology* **214**, 265–286.

Field, S. W. & Haggerty, S. E. (1994). Symplectite in upper mantle peridotites: development and implications for the growth of subsolidus garnet, pyroxene and spinel. *Contributions to Mineralogy and Petrology* **118**, 138–156.

Froitzheim, N., Jahn-Awe, S., Frei, D., Wainwright, A. N., Maas, R., Georgiev, N., Nagel, T. J. & Pleuger, J. (2014). Age and composition of meta-ophiolite from the Rhodope Middle Allochthon (Satovcha, Bulgaria): A test for the maximum-allochthony hypothesis of the Hellenides. *Tectonics* **32**, 1477–1500.

Frost, D. J. & McCammon, C. A. (2008). The redox state of Earth's mantle. *Annual Review of Earth and Planetary Sciences* **36**, 389–420.

Frost, D. J., Liebske, C., Langenhorst, F., McCammon, C. A., Trønnes, R. G. & Rubie, D. C. (2004). Experimental evidence for the existence of iron-rich metal in the Earth's lower mantle. *Nature* **248**, 409–412.

Girardeau, J. & Mercier, J. C. C. (1988). Petrology and textures of the ultramafic rocks of the Xigaze ophiolite: constraints for mantle structure beneath slow-spreading ridges. *Tectonophysics* **147**, 33–58.

Girardeau, J., Marcoux, J., Allègre, C., Bassoullet, J. P., Tang, Y., Xiao, X., Zao, Y. & Wang, X. (1984). Tectonic environment and geodynamic significance of the Neocimmerian Dongqiao ophiolite, Banggong–Nujiang Suture zone, Tibet. *Nature* **307**, 27–31.

Girardeau, J., Mercier, J. C. C. & Wang, X. (1985a). Petrology of the mafic rocks of the Xigaze ophiolite, Tibet: Implications for the genesis of the oceanic lithosphere. *Contributions to Mineralogy and Petrology* **90**, 309–321.

Girardeau, J., Mercier, J. C. C. & Zao, Y. (1985b). Structure of the Xigaze ophiolite, Yarlung Zangbo Suture Zone, southern Tibet, China: Genetic implications. *Tectonics* **4**, 267–288.

González-Jiménez, J. M., Griffin, W. L., Gervilla, F., Proenza, J. A., O'Reilly, S. Y. & Pearson, N. J. (2014a). Chromitites in ophiolites: How, where, when and why? Part I. A review and new ideas on the origin and significance of platinum-group minerals. *Lithos* **189**, 127–139.

González-Jiménez, J. M., Griffin, W. L., Proenza, J. A., Gervilla, F., O'Reilly, S. Y., Akbulut, M. & Pearson, N. J. (2014b). Chromitites in ophiolites: How, where, when and why? Part II. The crystallisation of chromitites. *Lithos* **189**, 140–158.

Gøpel, C., Allègre, C. J. & Xu, R.-H. (1984). Lead isotopic study of the Xigaze ophiolite (Tibet): the problem of the relationship between magmatites (gabbros, dolerites, lavas) and tectonites (harzburgites). *Earth and Planetary Science Letters* **69**, 301–310.

Green, D. H. & Falloon, T. J. (1998). Pyrolite: a Ringwood concept and its current expression. In: Jackson, I. (ed.) *The Earth's Mantle: Composition, Structure, and Evolution.* Cambridge University Press, pp. 311–378.

Green, H. W., II (2012). Record of deep upwelling in ophiolites: highly reduced environment containing very high pressure phases and nitrides from at least 300 km depth. *Abstracts, Geological Society of America Meeting*, **42**(**7**), 42–7.

Griffin, W. L. (2008). Major transformations reveal Earth's deep secrets. *Geology* **36**, 95–96.

Griffin, W. L., Graham, S., O'Reilly, S. Y. & Pearson, N. J. (2004). Lithosphere evolution beneath the Kaapvaal Craton. Re–Os systematics of sulfides in mantle-derived peridotites. *Chemical Geology* **208**, 89–118.

Griffin, W. L., Yang, J., Robinson, P. T., Howell, D., O'Reilly, S. Y. & Pearson, N. (2013). Going up or going down? Diamonds and super-reducing UHP assemblages in ophiolitic mantle. *Mineralogical Magazine* **77**, 1215.

Guilmette, C. (2005). Petrology, geochemistry and geochronology of highly foliated amphibolites from the ophiolitic mélange beneath the Yarlung Zangbo Ophiolites, Xigaze area, Tibet; Geodynamical implications. MSc thesis, Université Laval, Quebec, 191 pp.

Guilmette, C., Hebert, R., Dupuis, C., Wang, C. & Li, Z. (2008). Metamorphic history and geodynamic significance of high-grade metabasites from the ophiolitic mélange beneath the Yarlung Zangbo ophiolites, Xigaze area, Tibet. *Journal of Asian Earth Sciences* **32**, 423–437.

Guilmette, C., Hébert, R., Wang, C. S. & Villeneuve, M. (2009). Geochemistry and geochronology of the metamorphic sole underlying the Xigaze ophiolite, Yarlung Zangbo Suture Zone, south Tibet. *Lithos* **112**, 149–162.

Guilmette, C., Hebert, R., Dostal, J., Indares, A., Ullrich, T., Bedard, E. & Wang, C.S. (2012). The Co–Discovery of a dismembered metamorphic sole in the Saga ophiolitic mÕlange, South Tibet: Assessing an Early Cretaceous disruption of the Neo-Tethyan supra-subduction zone and consequences on basin closing. *Gondwana Research* **22**, 398–414.

Gupta, K. (1999). The Co–Mn–Ni (cobalt–manganese–nickel) system. *Journal of Phase Equilibria* **20**, 527–532.

Haggerty, S. E. & Sautter, V. (1990). Ultradeep (greater than 300 kilometers), ultramafic upper mantle xenoliths. *Science* **248**, 993–996.

Harrison, T. M., Yin, A., Grove, M. & Lovera, O. M. (2000). The Zedong window: A record of superposed Tertiary convergence in southeastern Tibet. *Journal of Geophysical Research* **105**, 19211–19231.

Hebert, R., Huot, F., Wang, C. & Liu, Z. (2003). Yarlung Zangbo ophiolites (Southern Tibet) revisited: Geodynamic implications from the mineral record. In: Dilek, Y. *& Robinson, P. (eds) Ophiolites in Earth History. Geological Society, London, Special Publications* **218**, 165–190.

Hebert, R., Bezard, R., Guilmette, C., Dostal, J., Wang, C. S. & Liu, Z. F. (2012). The Indus–Yarlung Zanbo ophiolites from Nanga Parbat to Namche Barwa syntaxes, southern Tibet: First synthesis of petrology, geochemistry, and geochronology with incidences on geodynamic reconstructions of Neo-Tethys. *Gondwana Research* **22**, 377–397.

Herzberg, C. (1992). Depth and degree of melting of komatiites. *Journal of Geophysical Research* **97**, 4521–4540.

Howell, D., Griffin, W. L., Yang, J., Gain, S., Stern, R. A., Huang, J.-X., Jacob, D. E., Xu, X., Stokes, A. J., O'Reilly, S. Y. & Pearson, N. J. (2015). Diamonds in ophiolites: Contamination or a new diamond growth environment? *Earth and Planetary Science Letters* **430**, 284–295.

Hu, X., Jansa, L. & Wang, C. (2008). Upper Jurassic–Lower Cretaceous stratigraphy in south-eastern Tibet: A comparison with the western Himalayas. *Cretaceous Research* **29**, 301–315.

Humphreys, E., Hessler, E., Dueker, K., Farmer, G. L., Erslev, E. & Atwater, T. (2003). How Laramide-age hydration of North American lithosphere by the Farallon slab controlled subsequent activity in the western United States. *International Geological Reviews* **45**, 575–595.

Irifune, T. (1985). Experimental study of the system $Mg_3Al_2Si_3O_{12}$–$Mg_3Cr_2Si_3O_{12}$ at high pressure and high

temperature. *Journal of the Faculty of Science, Hokkaido University* **21**, 417–451.

Jin, Z. M., Wu, Y., Xu, M. J., Fei, Y. W. & Robinson, P. T. (2014). How deep is the Tibetan chromitite: experimental study. In: *Abstracts, International Workshop on Ophiolites, Mantle Processes and Related Ore Deposits*, Beijing 2014. Chinese Academy of Geological Sciences (Abstracts, p. 24.).

Karato, I. (2008). *Deformation of Earth Materials: an Introduction to the Rheology of the Solid Earth*. Cambridge University Press, 463 pp.

Kawamoto, T. (2004). Hydrous phase stability and partial melt chemistry in H_2O-saturated KLB-1 peridotite up to the uppermost lower mantle conditions. *Physics of the Earth and Planetary Interiors* **143–144**, 387–395.

Kiefer, B., Stixrude, L. & Wentzcovitch, R. (1999). Normal and inverse ringwoodite at high pressures. *American Mineralogist* **84**, 288–293.

Kyono, A., Dera, P. K., Yamanake, T., Ikuta, D., Shu, J., Mao, H. & Hemley, R. J. (2009). In situ high-pressure single-crystal X-ray diffraction study of chromite. American Geophysical Union Fall Meeting 2009, abstract MR31B-1648.

Leier, A. L., Kapp, P., Gehrels, G. E. & DeCelles, P. G. (2007). Detrital geochronology of Carboniferous–Cretaceous strata in the Lhasa terrane, southern Tibet. *Basin Research* **19**, 361–378.

Levander, A., Bezada, M. J., Niu, F., Humphreys, E. D., Palomeras, I., Thurner, S. M., Masy, J., Schmitz, M., Gallart, J., Carbonell, J. & Miller, M. S. (2014). Subduction-driven recycling of continental margin lithosphere. *Nature* **515**, 253–257.

Li, J. F., Xia, B., Liu, L. W., Xu, L. F., He, G. S., Wang, H., Zhang, Y. Q. & Yang, Z. Q. (2009). SHRIMP U–Pb dating for the gabbro in Qunrang ophiolite, Tibet: The geochronology constraint for the development of eastern Tethys basin. *Geotectonica et Metallogenia* **33**, 294–298 (in Chinese with English abstract).

Liang, F., Xu, Z. & Zhao, J. (2014). *In-situ* moissanite in dunite: Deep mantle origin of mantle peridotite in Luobusa ophiolite, Tibet. *Acta Geologica Sinica* **88**, 517–521.

Litasov, K. D. & Ohtani, E. (2007). Effect of water on the phase relations in Earth's mantle and deep water cycle. In: Ohtani, E. (ed.) Advances in High-Pressure Mineralogy. *Geological Society of America, Special Papers* **421**, 115–156.

Liu, C. Z., Wu, F. Y., Wilde, S. A., Yu, L. J. & Li, J. L. (2010). Anorthitic plagioclase and pargasitic amphibole in mantle peridotites from the Yungbwa ophiolite (southwestern Tibetan Plateau) formed by hydrous melt metasomatism. *Lithos* **114**, 413–422.

Liu, C.-Z., Wu, F.-Y., Chu, Z.-Y., Ji, W.-Q., Yu, L.-J. & Li, J.-L. (2012). Preservation of ancient Os isotope signatures in the Yungbwa ophiolite (southwestern Tibet) after subduction modification. *Journal of Asian Earth Sciences* **53**, 38–50.

Liu, C.-Z., Zhang, C., Yang, L.-Y., Zhang, L.-L., Ji, W.-Q. & Wu, F.-Y. (2014). Formation of gabbronorites in the Purang ophiolite (SW Tibet) through melting of hydrothermally altered mantle along a detachment fault. *Lithos* **205**, 127–141.

Liu, F., Yang, J.-S., Dilek, Y., Xu, Z.-Q., Xu, X.-Z., Liang, F.-H., Chen, S.-Y. & Lian, D.-Y. (2015). Geochronology and geochemistry of basaltic lavas in the Dongbo and Purang opniolites of the Yarlung–Zangbo suture zone: Plume-influenced continental-margin-type oceanic lithosphere in southern Tibet. *Gondwana Research* **27**, 701–718.

Liu, L.-G. (1979). High-pressure phase transformations in baddeleyite and zircon, with geophysical implications. *Earth and Planetary Science Letters* **44**, 390–396.

Liu, W. L., Xia, B., Liu, H. F., Huang, W., Zhou, G. Q., Wei, D. L., Zhong, Y. & Ren, Y. Q. (2013). Zircon U–Pb dating of basalt from Zetang ophiolite in Tibet and its geological implications. *Geological Bulletin of China* **32**, 1356–1361 (in Chinese with English abstract).

Liu, Z., Li, Y., Xiong, F. H., Wu, D. & Liu, F. (2011). Petrology and geochronology of MOR gabbro in the Purang ophiolite of western Tibet, China. *Acta Petrologica Sinica* **27**, 3269–3279 (in Chinese with English abstract).

Malavieille, J., Lallemand, S. E., Dominguez, S., Deschamps, A., Lu, C.-Y., Liu, C.-S., Schnurle, P. & Crew, A. S. (2002). Arc–continent collision in Taiwan: new marine observations and tectonic evolution. In: Byrne, T.B. & Liu, C.S. (eds) Geology and Geophysics of an Arc-Continent collision, Taiwan, Republic of China. *Geological Society of America, Special Papers* **358**, 189–213.

Malpas, J., Zhou, M.-F., Robinson, P. T. & Reynolds, P. (2003). Geochemical and geochronological constraints on the origin and emplacement of the Yarlung Zangbo ophiolites, southern Tibet. In: Dilek, Y. & Robinson, P. (eds) *Ophiolites in Earth History. Geological Society, London, Special Publications* **218**, 191–206.

Manga, M. (1996). Mixing of heterogeneities in the mantle: Effect of viscosity differences. *Geophysical Research Letters* **23**, 403–406.

McCammon, C. M. (2005). The paradox of mantle redox. *Science* **308**, 807–808.

McDermid, I. R. C., Aitchison, J. C., Davis, A. M., Harrison, T. M. & Grove, M. (2002). The Zedong terrane: a Late Jurassic intra-oceanic magmatic arc within the Yarlung–Tsangpo suture zone, southeastern Tibet. *Chemical Geology* **187**, 267–277.

McGowan, N. M., Griffin, W. L., González-Jiménez, J. M., Belousova, E. A., Afonso, J., Shi, R., McCammon, C. A., Pearson, N. J. & O'Reilly, S. Y. (2015). Tibetan chromitites: Excavating the slab graveyard. *Geology* **43**, 179–182.

Medaris, L. G., Jr, Fournelle, J. H., Wang, H. F. & Jelínek, E. (1997). Thermobarometry and reconstructed chemical compositions of spinel–pyroxene symplectites: Evidence for pre-existing garnet in lherzolite xenoliths from Czech Neogene lavas. *Russian Geology and Geophysics* **38**, 277–286.

Melcher, F., Grum, W., Simon, G. H., Thalhammer, T. V. & Stumpfl, E. F. (1997). Petrogenesis of giant chromite deposits of Kempirsai, Kazakhstan: a study of solid and fluid inclusions in chromite. *Journal of Petrology* **38**, 1419–1458.

Metcalfe, I. (1996). Gondwanaland dispersion, Asian accretion and evolution of eastern Tethys. *Australian Journal of Earth Sciences* **43**, 605–623.

Moghadam, H. S., Li, X.-H., Ling, X.-X., Stern, R. J., Khedr, M. Z., Chiaradia, M., Ghorbani, G., Arai, S. & Tamura, A. (2015). Devonian to Permian evolution of the Paleo-Tethys Ocean: new evidence from U–Pb zircon dating and Sr–Nd–Pb isotopes of the Darrehanjir–Mashad 'ophiolites', NE Iran. *Gondwana Research* **28**, 781–799.

Moresi, L., Betts, P. G., Miller, M. S. & Cayley, R. A. (2014). Dynamics of continental accretion. *Nature* **508**, 245–248.

Morishita, T. & Arai, S. (2003). Evolution of spinel–pyroxene symplectite in spinel lherzolites from the Horoman Complex, Japan. *Contributions to Mineralogy and Petrology* **144**, 509–522.

Murayama, J. K., Nakai, S., Kato, M. & Kumazawa, M. (1986). A dense polymorph of $Ca_3(PO_4)_2$: a high pressure phase of apatite decomposition and its geochemical significance. *Physics of the Earth and Planetary Interiors* **44**, 293–303.

Murphy, M. A., Yin, A. & Harrison, T. M. (1997). Did the Indo-Asian collision alone create the Tibetan Plateau? *Geology* **25**, 719–722.

Nicolas, A., Girardeau, J., Marcoux, J., Dupre, B., Wang, X., Cao, Y., Zheng, H. & Xiao, X. (1981). The Xigaze ophiolite (Tibet): a peculiar oceanic lithosphere. *Nature* **294**, 414–417.

Niu, X. L., Yang, J. S., Dilek, Y., Xu, J. F., Li, J., Chen, S. Y., Feng, G. Y., Liu, F., Xiong, F. H. & Liu, Z. (2015). Petrological and Os isotopic constraints on the origin of the Dongbo peridotite massif, Yarlung Zangbo Suture Zone, Western Tibet. *Journal of Asian Earth Sciences* **110**, 72–84.

O'Neill, H. St. C. & Navrotsky, A. (1983). Simple spinels: crystallographic parameters, cation radii, lattice energies and cation distribution. *American Mineralogist* **89**, 181–194.

O'Neill, H. St. C., Rubie, D. C., Geiger, C. A., Ross, C. R., II, Siefert, F & Woodland, A. B. (1993). Ferric iron in the upper mantle and in Transition Zone assemblages: Implications for relative oxygen fugacities in the mantle. In: Takahashi, E., Jeanloz, R. & Rubie, D. (eds) Evolution of the Earth and planets. *American Geophysical Union, Geophysical Monograph* **74**, 73–88.

Ono, S., Funakoshi, K., Nakajima, Y., Tange, Y. & Katsura, T. (2003). *Geology Fields*. Okoyama University, pp. 1–22.

Pearce, J. A. & Deng, W. M. (1988). The ophiolites of the Tibet Geotraverses, Lhasa to Golmud (1985) and Lahasa to Kathmandu (1986). *Philosophical Transactions of the Royal Society of London, Series A* **327**, 215–238.

Pearson, D. G., Davies, G. R. & Nixon, P. H. (1993). Geochemical constraints on the petrogenesis of diamond facies pyroxenites from the Beni Boussera peridotitic massif, North Morocco. *Journal of Petrology* **34**, 125–172.

Piccardo, G. B., Zanetti, A. & Müntener, O. (2007). Melt/peridotite interaction in the Lanzo South peridotite: field, textural and geochemical evidence. *Lithos* **94**, 181–209.

Pritchard, H. M., Barnes, S. J., Godel, B., Reddy, S. M., Vukmanovic, Z., Halfpenny, A., Nearly, C. R. & Fisher, P. C. (2015). The structure and origin of nodular chromitite from the Troodos ophiolite, Cyprus, revealed using high-resolution X-ray computed tomography and electron backscatter diffraction. *Lithos* **218–219**, 87–98.

Proenza, J. A., Gervilla, F., Melgarejo, J. C. & Bodinier, J. L. (1999). Al- and Cr- rich chromitites from the Mayari–Baracoa Ophiolite Belt (eastern Cuba): consequence of interaction between volatile-rich melts and peridotite in suprasubduction mantle. *Economic Geology* **94**, 547–566.

Rampone, E., Romairone, A., Abouchami, W., Piccardo, G. B. & Hofmann, A. W. (2005). Chronology, petrology and isotope geochemistry of the Erro–Tobbio peridotites (Ligurian Alps, Italy): Records of late Palaeozoic lithospheric extension. *Journal of Petrology* **46**, 799–827.

Reid, A. F. & Ringwood, A. E. (1969). Newly observed high-pressure transformations in Mn_3O_4, $CaAl_2O_4$ and $ZrSiO_4$. *Earth and Planetary Science Letters* **6**, 205–214.

Ren, Y., Chen, F., Yang, J. & Gao, Y. (2008). Exsolutions of diopside and magnetite in olivine from mantle dunite, Luobusa ophiolite, Tibet, China. *Acta Geologica Sinica* **82**, 377–384.

Robin-Popieul, C. C. M., Arndt, N. T., Chauvel, C., Byerly, G. R., Sobolev, A & Wilson, A. (2012). A new model for Barberton komatiites: Deep critical melting with high melt retention. *Journal of Petrology* **53**, 2191–2229.

Robinson, P. T., Bai, W.-J., Malpas, J., Yang, J.-S., Zhou, M.-F., Fang, Q.-S., Hu, X.-F., Cameron, S. & Staudigel, H. (2004). Ultra-high pressure minerals in the Luobusa ophiolite, Tibet, and their tectonic implications. In: Malpas, J., Fletcher, C. J. N., Ali, J. R. & Aitchison, J. C. (eds) *Aspects of the Tectonic Evolution of China. Geological Society, London, Special Publications* **226**, 247–271.

Robinson, P. T., Trumbull, R. B., Schmitt, Z., Yang, J.-S., Li, J.-W., Zhou, M.-F., Erzinger, J., Dare, S. & Xiong, F. (2015). The origin and significance of crustal minerals in ophiolitic chromitites and peridotites. *Gondwana Research* **27**, 486–506.

Rohrbach, A., Ballhaus, C., Golla-Schindler, U., Ulmer, P., Kamenetsky, V. S. & Kuzmin, D. V. (2007). Metal saturation in the upper mantle. *Nature* **449**, 456–458.

Roup, A., Kalmanovitch, E., Baykov, Y. & Toledo, V. (2009). Shefa Yamim moissanite discovery in Israel. *Abstracts, Israel Geological Society Meeting* **2009**, pp. 111.

Ruskov, T., Spirov, I., Georgieva, M., Yamamoto, S., Green, H. W., McCammon, C. A. & Dobrzhinetskaya, L. F. (2010). Møssbauer spectroscopy studies of the valence state of iron in chromite from the Luobusa massif of Tibet: implications for a highly reduced deep mantle. *Journal of Metamorphic Geology* **28**, 551–560.

Satsukawa, T., Griffin, W. L., Piazolo, S. & O'Reilly, S. Y. (2015). Messengers from the deep: Fossil wadsleyite–chromite microstructures from the Mantle Transition Zone. *Scientific Reports* **5**, 16484.

Sautter, V., Haggerty, S. E. & Field, S. (1991). Ultradeep (>300 kilometers) ultramafic xenoliths: Petrological evidence from the transition zone. *Science* **252**, 827–830.

Scholl, D. W. & von Huene, R. (2007). Crustal recycling at modern subduction zones applied to the past—Issues of growth and preservation of continental basement crust, mantle geochemistry, and supercontinent reconstruction. In: Hatcher Jr, R. D., Carlson, M. P., McBride, J. H. & Martinez Catalan, J. R. (eds) 4-D framework of continental crust. *Geological Society of America, Memoirs* **200**, 9–32.

Shi, R., Alard, O., Zhi, X., O'Reilly, S. Y., Pearson, N. J., Griffin, W. L., Zhang, M. & Chen, X. (2007). Multiple events in the Neo-Tethyan oceanic upper mantle: evidence from Ru–Os–Ir alloys in the Luobusa and Dongqiao ophiolitic podiform chromitites, Tibet. *Earth and Planetary Science Letters* **261**, 33–48.

Shi, R., Griffin W. L., O'Reilly, S. Y., Huang, Q., Zhang, X., Liu, D., Zhi, X., Xia, Q. & Ding, L. (2012a). Melt/mantle mixing produces podiform chromite deposits in ophiolites: Implications of Re–Os systematics in the Dongqiao Neo-Tethyan ophiolite, northern Tibet. *Gondwana Research* **21**, 194–206.

Shi, R., Huang, Q., Liu, D., Fan, S., Zhang, X., Ding, L., Griffin, W. L. & O'Reilly, S. Y. (2012b). Recycling of ancient sub-continental lithospheric mantle: Constraints on the genesis of the ophiolitic podiform chromitites. *Geological Review* **58**, 643–652 (in Chinese with English abstract).

Shimuzu, Y., Arai, S., Morishita, T. & Ishida, Y. (2008). Origin and significance of spinel–pyroxene symplecitite in lherzolite xenoliths from Tallante, SE, Spain. *Mineralogy and Petrology* **94**, 27–43.

Shirey, S. B. & Walker, R. J. (1998). The Re–Os isotope system in cosmochemistry and high-temperature geochemistry. *Annual Review of Earth and Planetary Sciences* **26**, 423–500.

Smith, D. (1977). The origin and interpretation of spinel–pyroxene clusters in peridotite. *Journal of Geology* **85**, 476–482.

Sobolev, S. V. & Babeyko, A. Y. (2005). What drives orogeny in the Andes? *Geology* **33**, 617–620.

Takahashi, N. (2001). Origin of plagioclase lherzolite from the Nikanbetsu peridotite complex, Hokkaido, northern Japan: implications for incipient melt migration and segregation in the partial molten upper mantle. *Journal of Petrology* **42**, 87–105.

Toledo, V., Griffin, W. L., Gain, S. E. M., O'Reilly, S. Y., Jacob, D. & Pearson, N. J. (2015). Corundum, moissanite and super-reducing conditions in the upper mantle beneath the Lower (southern) Galilee (Israel). *Abstracts, Israel Geology Society Meeting* **2015**, 145.

Tubía, J. M., Cuevas, J. & Esteban, J. J. (2004). Tectonic evidence in the Ronda peridotites, Spain, for mantle diapirism related to delamination. *Geology* **32**, 941–944.

Ulmer, P. & Trommsdorff, V. (1995). Serpentine stability to mantle depths and subduction-related magmatism. *Science* **268**, 858–861.

Vissers, R. L. M., Platt, J. P. & van der Wal, D. (1995). Late orogenic extension of the Betic Cordillera and the Alboran Domain: A lithospheric view. *Tectonics* **14**, 786–803.

Wakabayashi, J. & Dilek, Y. (2000). Spatial and temporal relationships between ophiolites and their metamorphic soles: A test of models of forearc ophiolite genesis. In: Dilek, Y., Moores, E. M., Elthon D. & Nicholas, A. (eds) *Ophiolites and Oceanic Crust: New Insights from Field Studies and the Ocean Drilling Program. Geological Society of America, Special Papers* **349**, 53–64.

Walker, R. J., Horan, M. F., Morgan, J. W., Becker, H., Grossman, J. N. & Rubin, A. E. (2002). Comparative ^{187}Re–^{187}Os systematics of chondrites: Implications regarding early solar system processes. *Geochimica et Cosmochimica Acta* **66**, 4187–4201.

Wang, C., Li, X., Liu, Z., Li, Y., Jansa, L., Dai, J. & Wei, Y. (2012). Revision of the Cretaceous–Paleogene stratigraphic framework, facies architecture and provenance of the Xigaze forearc basin along the Yarlung Zangbo suture zone. *Gondwana Research* **22**, 415–433.

Wang, J.-G., Hu, X.-M., Wu, F.-Y. & Jansa, L. (2010). Provenance of the Liuqu comglomerate in southern Tibet: A Paleogene erosional record of the Himalayan–Tibetan orogeny. *Sedimentary Geology* **231**, 74–84.

Wang, R., Xia, B., Zhou, G. Q., Zhang, Y. Q., Yang, Z. Q., Li, W. Q., Wei, D. L., Zhong, L. F. & Xu, L. F. (2006). SHRIMP zircon U–Pb dating for gabbro from the Tiding ophiolite in Tibet. *Chinese Science Bulletin* **51**, 1776–1779.

Wang, X. B., Bao, P. S. & Xiao, X. C. (1987). *Ophiolites of the Yarlung Zangbo River, Xizang*. Publishing House of Surveying and Mapping.

Wei, D. L., Xia, B., Zhou, G. Q., Wang, R., Zhong, L. F. & Wan, S. K. (2006). Sm–Nd isochron age of Zedang Ophiolite in Tibet and its significance. *Acta Geoscientica Sinica* **27**, 31–34.

Wu, F. Y., Ji, W. Q., Liu, C. Z. & Chung, S. L. (2010). Detrital zircon U–Pb and Hf isotopic data from the Xigaze fore-arc basin: Constraints on Transhimalayan magmatic evolution in southern Tibet. *Chemical Geology* **271**, 13–25.

Wu, F. Y., Liu, C. Z., Zhang, L. L., Zhang, C., Wang, J. G., Ji, W. Q. & Liu, X. C. (2014). Yarlung Zangbo ophiolites: a critical updated view. *Acta Petrologica Sinica* **30**, 293–325 (in Chinese with English abstract).

Wu, Y., Xu, M., Fei, Y. & Jin, Z. (2011). Phase relations in chromite + SiO^2 system at high pressure and high temperature and implications for the origin of coesite bearing chromite. *American Geophysical Union Fall Meeting 2011*, abstract T53E-07.

Xia, B., Yu, H.-X., Chen, G.-W., Qi, L., Zhao, T.-P. & Zhou, M.-F. (2003). Geochemistry and tectonic environment of the Dagzhuka ophiolite in the Yarlung–Zangbo suture zone, Tibet. *Geochemical Journal* **37**, 311–324.

Xia, B., Li, J. F., Liu, L. W., Xu, L. F., He, G. S., Wang, H., Zhang, Y. Q. & Yang, Z. Q. (2008). SHRIMP U–Pb dating for diabase in Sangsang ophiolite, Xizang, China: Geochronological constraint for development of eastern Tethys basin. *Geochimica* **37**, 399–403 (in Chinese with English abstract).

Xiong, F. H., Yang, J. S., Liang, F. H., Ba, D. Z., Zhang, J., Xu, X. Z., Li, Y. & Liu, Z. (2011). Zircon U–Pb ages of the Dongbo ophiolite in the western Yarlung Zangbo suture zone and their geological significance. *Acta Petrologica Sinica* **27**, 3223–3238 (in Chinese with English abstract).

Xiong, F. H., Yang, J., Robinson, P. T., Xu, X., Liu, Z., Li, Y., Li, J & Chen, S. (2015). Origin of podiform chromitite, a new model based on the Luobusa ophiolite, Tibet. *Gondwana Research* **27**, 525–542.

Xiong, Q. (2015). Shenglikou and Zedang peridotite massifs, Tibet (China): Upper mantle processes and geodynamic significance. PhD thesis, Macquarie University, Sydney, NSW, 268 pp.

Xiong, Q., Griffin, W. L., Zheng, J. P., O'Reilly, S. Y., Pearson, N. J., Xu, B. & Belousova, E. A. (2016). Southward trench migration at ~130–120 Ma caused accretion of the Neo-Tethyan forearc lithosphere in Tibetan ophiolites. *Earth and Planetary Science Letters* **438**, 57–65.

Xu, M.-J. & Jin, Z.-M. (2010). Deformation microstructures of mantle peridotite from Luobusha ophiolite, Tibet, China and its geological implication. *Geological Bulletin of China* **29**, 1795–1803.

Xu, X., Yang, J., Chen, S., Fang, Q., Bai, W. & Ba, D. (2009). Unusual mantle mineral group from chromitite orebody Cr-11 in Luobusa ophiolite of Yarlung–Zangbo Suture Zone, Tibet. *Journal of Earth Science* **20**, 284–302.

Xu, X., Yang, J., Ba, D., Guo, G., Robinson, P. T. & Li, J. (2011). Petrogenesis of the Kangjinla peridotite in the Luobusa ophiolite, Southern Tibet. *Journal of Asian Earth Sciences* **42**, 553–568.

Xu, X., Yang, J., Robinson, P. T., Xiong, F., Ba, D. & Guo, G. (2015). Origin of ultrahigh pressure and highly reduced minerals in podiform chromitites and associated mantle peridotites of the Luobusa ophiolite, Tibet. *Gondwana Research* **27**, 686–700.

Yamamoto, H., Yamamoto, S., Kaneko, Y., Terabayashi, M., Komiya, T., Katayama, I. & Iizuka, T. (2007). Imbricate structure of the Luobusa Ophiolite and surrounding rock units, southern Tibet. *Journal of Asian Earth Sciences* **29**, 296–304.

Yamamoto, S., Komiya, T., Hirose, K. & Maruyama, S. (2009). Coesite and clinopyroxene exsolution lamellae in chromites: *In-situ* ultrahigh-pressure evidence from podiform chromitites in the Luobusa ophiolite, southern Tibet. *Lithos* **109**, 314–322.

Yamamoto, S., Komiya, T., Yamamoto, H., Kaneko, Y., Terabayashi, M., Katayama, I., Iizuka, T., Maruyama, S., Yang, J., Kon, Y. & Hirata, T. (2013). Recycled crustal zircons from podiform chromitites in the Luobusa ophiolite, southern Tibet. *Island Arc* **22**, 89–103.

Yang, F. Y., Kang, Z. Q. & Liu, S. C. (1981). A new octahedral pseudomorph of lizardite and its origin. *Acta Mineralogica Sinica* **1**, 52–54 (in Chinese with English abstract).

Yang, J.-S., Dobrzhinetskaya, L. F., Bai, W. J., Fang, Q. S., Robinson, P. T., Zhang, J. F. & Green, H. W., II (2007). Diamond- and coesite-bearing chromitites from the Luobusa ophiolite, Tibet. *Geology* **35**, 875–878.

Yang, J. S., Robinson, P. T. & Dilek, Y. (2014). Diamonds in ophiolites. *Elements* **10**, 127–130.

Yang, J. S., Meng,. F., Xu, S., Robinson, P. T., Dilek, Y., Makeyev, A. B., Wirth, R., Wiedenbeck, M. & Cliff, J. (2015). Diamonds, native elements and metal alloys from chromitites of the Ray-Iz ophiolite of the Polar Urals. *Gondwana Research* **27**, 459–485.

Zhang, S. Q., Mahoney, J. J., Mo, X. X., Ghazi, A. M., Milani, L., Crawford, A. J., Guo, T. Y. & Zhao, Z. D. (2005). Evidence for a widespread Tethyan upper mantle with Indian-Ocean-type isotopic characteristics. *Journal of Petrology* **46**, 829–858.

Zhong, L. F., Xia, B., Zhou, G. Q., Zhang, Y. Q., Wang, R., Wei, D. L. & Yang, Z. Q. (2006). SHRIMP age determination of the diabase in Luobusa ophiolite, Southern Xizang (Tibet). *Geological Review* **52**, 224–229 (in Chinese with English abstract).

Zhou, M. F., Robinson, P. T., Malpas, J. & Li, Z. (1996). Podiform chromitites in the Luobusa ophiolite (southern Tibet): implications for melt–rock interaction and chromite segregation in the upper mantle. *Journal of Petrology* **37**, 3–21.

Zhou, M. F., Robinson, P. T., Malpas, J., Edwards, S. J. & Qi, L. (2005). REE and PGE geochemical constraints on the formation of dunites in the Luobusa ophiolite, Southern Tibet. *Journal of Petrology* **46**, 615–639.

Zhou, M. F., Robinson, P. T., Su, B. X., Gao, J. F., Li, J. Q., Yang, J. S. & Malpas, J. (2014). Compositions of chromite, associated minerals, and parental magmas of podiform chromite deposits: the role of slab contamination of asthenospheric melts in suprasubduction zone environments. *Gondwana Research* **26**, 262–283.

Zhou, S., Mo, X. X., Mahoney, J. J., Zhang, S. Q., Guo, T. Y. & Zhao, Z. D. (2002). Geochronology and Nd and Pb isotope characteristics of gabbro dikes in the Luobusha ophiolite, Tibet. *Chinese Science Bulletin* **47**, 143–146.

Ziabrev, S. V., Aitchison, J. C., Ba, D., Davis, A. M., Luo, H. & Malpas, J. (1999). Radiolarian biostratigraphy of supra-ophiolite sequences in the Xigaze area, Yarlung–Tsangpo suture, southern Tibet (preliminary report). *Radiolaria* **17**, 13–19.

Ziabrev, S. V., Aitchison, J. C., Abrajevitch, A., Ba, D., Davis, A. M. & Luo, H. (2003). Precise radiolarian age constraints on the timing of Dazhuqu terrane ophiolite generation and sedimentation, Yarlung–Tsangpo suture zone, Tibet. *Journal of the Geological Society, London* **160**, 591–600.